이학박사 학위논문

Exploration of Neurodegenerative Diseases Mimicking Alzheimer's Diseases: Volume and Texture Analysis of Magnetic Resonance Imaging

알츠하이머병과 유사한 신경 퇴행성 질환의 탐구: 자기공명영상의 부피 및 텍스처 분석

2025년 02월

서울대학교 대학원

뇌인지과학과

권 민 정

Exploration of Neurodegenerative Diseases Mimicking Alzheimer's Diseases: Volume and Texture Analysis of Magnetic Resonance Imaging

알츠하이머병과 유사한 신경 퇴행성 질환의 탐구: 자기공명영상의 부피 및 텍스처 분석

지도 교수 김 기 웅

이 논문을 이학박사학위논문으로 제출함

2025년 1월

서울대학교 대학원

뇌인지과학과

권 민 정

권민정의 이학박사 학위논문을 인준함

2025년 1월

위 원 장	김의태	(인)
부위원장	김기웅	(인)
위 원	이상아 Lee Sang Ah	(인)
위 원	최형진	(인)
위 원	박준혁	(인)

Abstract

Exploration of Neurodegenerative Diseases Mimicking Alzheimer's Diseases: Volume and Texture Analysis of Magnetic Resonance Imaging

Min Jeong Kwon

Department of Brain and Cognitive Sciences

Seoul National University

Background and Objectives: Semantic dementia (SD) and suspected non-Alzheimer's disease pathophysiology (SNAP) are neurodegenerative conditions distinct from Alzheimer's disease (AD), yet they share overlapping clinical and neuroimaging features, complicating early diagnosis and treatment. While AD diagnostic tools, such as amyloid PET imaging and molecular biomarkers, have advanced, equivalent tools for SD and SNAP remain underdeveloped. Structural MRI is a valuable tool; however, traditional volume-based analyses are insufficient for detecting subtle neurodegenerative changes. Texture analysis, which quantifies microstructural changes in brain tissue, may address this gap by providing a more nuanced understanding of disease-specific neurodegenerative patterns. This study aims to address gaps in the differentiation of SD and SNAP from AD and NC by utilizing structural MRI-based brain volume and texture metrics. Specifically, the

study seeks to (1) identify distinct neurodegenerative patterns in SD and SNAP through comprehensive evaluation of structural and microstructural changes; and (2) enhance diagnostic accuracy by integrating volume and texture features, thereby improving the differentiation of SD and SNAP from NC and AD compared to single-modality approaches.

Methods: This study analyzed structural MRI data to differentiate neurodegenerative patterns among SD, SNAP, and AD. Study 1 included 30 SD patients, 60 age-, sex-, and education-matched AD patients, and 60 normal controls (NC) from the Korean Longitudinal Study on Cognitive Aging and Dementia (KLOSCAD). Study 2 included 502 participants: 288 from a dementia clinic and 214 KLOSCAD participants. Participants were classified into NC (A-N-), AD (A+N+), and SNAP (A-N+) groups based on amyloid beta deposition and neurodegeneration markers using 18F-florbetaben PET and MRI.

We measured brain volumes using FreeSurfer from 3D T1-weighted brain MRI. We extracted texture features through a three-step pre-processing procedure that included histogram normalization, intensity normalization relative to cerebrospinal fluid (CSF), and rescaling grey-level values to a uniform range. We calculated texture metrics using grey-level co-occurrence matrices (GLCMs), with "contrast" reflecting local grey-level variations and spatial distributions within specific brain regions.

We developed logistic regression models for classification using volume and texture features, proposing a composite model combining significant features from both modalities. Model performance was evaluated through receiver operating characteristic (ROC) curve analysis, comparing areas under the curve (AUC). Statistical analyses, including ANCOVA for group comparisons, were conducted using SPSS and MedCalc. Significance was set at $P < 0.05$.

Results: In Study 1, SD demonstrated distinct patterns of cognitive impairment and neurodegeneration compared to NC and AD. SD patients exhibited significant atrophy in the temporal pole, with corresponding microstructural changes revealed by texture analysis. Logistic regression models showed that texture features in the temporal pole and hippocampus effectively distinguished SD from NC and AD. Composite models combining volume and texture metrics improved classification accuracy, emphasizing the role of microstructural alterations in SD.

In Study 2, SNAP and AD demonstrated distinct patterns of structural and microstructural changes. Texture analysis revealed elevated heterogeneity in subcortical regions, particularly in the thalamus, which distinguished SNAP from AD. Logistic regression models identified frontal and subcortical texture features as key discriminators for SNAP. Composite models integrating volume and texture metrics enhanced diagnostic performance, underscoring the utility of texture analysis in detecting subtle neurodegenerative differences in SNAP.

Conclusion: This study demonstrates the value of combining texture and volume

analysis in differentiating neurodegenerative conditions like semantic dementia (SD) and suspected non-Alzheimer's disease pathophysiology (SNAP) from Alzheimer's disease (AD). Volume analysis captures structural atrophy, while texture analysis detects subtle microstructural changes, offering complementary insights into disease-specific mechanisms. Integrating these metrics enhances early diagnosis and differentiation, providing a critical advancement in neuroimaging for dementia and related conditions.

Keywords: Alzheimer's disease**,** Semantic dementia**,** Suspected Non-Alzheimer's Disease Pathophysiology**,** magnetic resonance imaging, volume, texture

Student number: 2020-31019

Contents

List of Tables

List of Figures

List of Supplementary materials

List of Abbreviations

AD	Alzheimer's disease
AUC	Area under the (receiver operator characteristic) curve
BNT	15-item Boston Naming Test
CPT	Constructional Praxis Test
CRT	Constructional Recall Test
DST	Digit Span Test
FAB	Frontal Assessment Battery
GLCM	Gray-level co-occurrence matrix
KLOSCAD	Korean Longitudinal Study on Cognitive Aging and Dementia
MCI	Mild Cognitive Impairment
MMSE	Mini Mental Status Examination
MRI	Magnetic Resonance Imaging
NC	Normal cognition
NFT	Neurofibrillary tangle
PET	Positron emission tomography
ROC	Receiver operator characteristic
ROI	Region of interest
T	Tesla
T1w	Longitudinal relaxation time / T1-weighted
SNUBH	Seoul National University Bundang Hospital
TMT-A	Trail Making Test A

TMT-B	Trail Making Test B
VFT	Verbal Fluency Test
WLMT	Word List Memory Test
WLRT	Word List Recall Test
WLRcT	Word List Recognition Test
3D	Three-dimensional

1. Introduction

1.1. Study Background

Dementia encompasses a spectrum of neurodegenerative disorders that pose significant diagnostic and therapeutic challenges. Alzheimer's disease (AD), the most prevalent form of dementia, accounts for 60–70% of cases and is characterized by medial temporal lobe atrophy observable on magnetic resonance imaging (MRI). However, other conditions, such as semantic dementia (SD) and suspected non-Alzheimer's disease pathophysiology (SNAP), have been increasingly recognized as clinically and pathologically distinct entities. Although these non-Alzheimer's diseases (non-AD) are less common, they hold substantial clinical and research importance due to their unique neurodegenerative trajectories, distinct pathological mechanisms, and differential responses to treatment. Despite these distinctions, research on non-AD conditions remains limited. Many non-AD diseases exhibit similar atrophy patterns on MRI and clinical symptoms to AD, despite having different underlying causes. This overlap complicates differential diagnosis, particularly in the early stages, and may lead to misdiagnoses. Therefore, clearly distinguishing AD from non-AD is critical for effective diagnosis and treatment.

SD, a variant of frontotemporal lobar degeneration (FTLD), predominantly affects the anterior temporal lobe and is characterized by a progressive loss of

semantic knowledge, impaired object recognition, and deficits in word comprehension. SD accounts for approximately 20% of FTLD cases, with an estimated prevalence of 3–5 cases per 100,000 in individuals aged 45–64 years. (Ratnavalli et al., 2002) Its primary pathological hallmark is the accumulation of tau protein aggregates (tauopathy) within neurons, glial cells, and neurites. In some cases, SD is associated with TDP-43 pathology, particularly in patients with more extensive cortical involvement. (David Neary et al., 1998; Snowden et al., 2004) These pathological changes lead to a gradual disconnection of the semantic network, starting in the anterior temporal lobe and often spreading to adjacent regions as the disease progresses.

In contrast, SNAP is characterized by evidence of neurodegeneration without amyloid beta (Aβ) pathology, as determined through PET imaging or biomarker assessments. Introduced by the NIA-AA in 2012, SNAP encompasses non-AD conditions and is marked by abnormal levels of neurodegeneration markers (N+) in the absence of Aβ markers (A-). (Jack Jr et al., 2018a; Jack Jr et al., 2012) SNAP accounts for approximately 23% of older individuals with normal cognition (NC) and up to 25% of those with mild cognitive impairment (MCI). Unlike AD, which is driven by amyloid pathology, SNAP follows a trajectory influenced by non-amyloid mechanisms such as tauopathy, TDP-43 pathology, or alpha-synucleinopathy, leading to neurodegeneration in key brain regions.

The clinical significance of SD and SNAP lies in their early overlap with

AD symptoms, particularly due to their shared neurodegenerative involvement of the temporal lobe. In the early stages, both disorders may present with memory impairment, language deficits, or other cognitive symptoms resembling AD, making differential diagnosis challenging. (Landin-Romero et al., 2016; Snowden et al., 2018) However, as the diseases progress, SD and SNAP diverge in their symptomatology and underlying pathophysiology. (Mummery et al., 2000) SD is associated with severe atrophy in the anterior temporal lobe, reflecting its selective impact on semantic processing circuits, whereas SNAP shows focal atrophy in memory-related regions, consistent with its non-amyloid neurodegenerative process. Therefore, the early differentiation of these diseases from AD is of significant importance for predicting the course of the disease and providing tailored management and disease education.

While AD benefits from advanced diagnostic tools such as amyloid PET imaging and molecular biomarkers in blood or cerebrospinal fluid (CSF), equivalent tools for SD and SNAP are lacking. In AD, these biomarkers facilitate the detection of pathogenic proteins even at preclinical stages, providing valuable insights into the progression of neurodegeneration. (Janelidze et al., 2016; Klunk et al., 2004) However, due to the heterogeneous nature and lack of specific in vivo molecular biomarkers of SD and SNAP, structural imaging techniques such as MRI play a pivotal role in diagnosing and monitoring disease progression in SD and SNAP. Among MRI-based biomarkers, brain volume measurements have

traditionally been utilized to evaluate macroscopic alterations associated with neurodegeneration. However, volume measures alone are limited in their ability to detect subtle or early neurodegenerative changes, particularly when distinguishing SD and SNAP from AD.

Texture analysis has emerged as a promising neuroimaging technique to address these limitations. Unlike volumetric measures, texture analysis quantifies microstructural changes in brain tissue by examining the interrelationships between voxels, making it more sensitive to subtle changes in gray matter. (Lee et al., 2021) (Eickhoff et al., 2005) In previous studies, texture changes were shown to precede volume changes in AD, highlighting its potential as an early diagnostic tool. (Lee et al., 2020) For instance, increased texture contrast, which reflects greater intensity heterogeneity, can indicate significant microstructural abnormalities related to tau or TDP-43 protein accumulation. (Does, 2018; Hodges et al., 2010; Josephs et al., 2011; Landin-Romero et al., 2016; Rohrer et al., 2011) In SD, texture analysis captures disruptions in semantic processing circuits within the anterior temporal lobe, while in SNAP, it detects localized microstructural changes in regions such as the hippocampus and posterior cingulate cortex that are not apparent with volumetric measures alone. These findings suggest that texture analysis provides a more nuanced understanding of neurodegenerative processes, enabling improved differentiation of SD and SNAP from AD.

The objective of this study is to elucidate the unique neurodegenerative

patterns and diagnostic challenges associated with SD and SNAP through advanced microstructural MRI analysis along with conventional macrostructural analysis. Specifically, the objectives are to:

1. Characterize distinct neurodegenerative patterns: Identify disease-specific patterns of macroscopic changes (i.e., volume) and microscopic changes (i.e., texture) in the brains of SD and SNAP, emphasizing their differentiation from AD and NC.

2. Enhance accuracy of diagnosis and differential diagnosis: Develop and validate composite diagnostic models that integrate volume and texture features. These models demonstrate superior performance in distinguishing SD and SNAP from AD and NC compared to single-modality approaches.

3. Advance early detection strategies: Highlight the potential of texture analysis as an early diagnostic tool. This is accomplished by uncovering subtle microstructural alterations in key brain regions before significant volumetric changes occur.

By addressing these objectives, the study seeks to refine the diagnostic framework for SD and SNAP, providing a foundation for improved clinical decision-making and targeted therapeutic strategies.

1.2. Study Hypotheses

Neurodegenerative diseases such as SD and suspected SNAP exhibit

clinical and neuroimaging features that are similar to those of AD. Despite these similarities, each condition follows distinct pathological mechanisms that result in unique patterns of neurodegeneration. The central tenet of this study is the hypothesis that macrostructural and microstructural analyses are complementary in refining the differential diagnosis of neurodegenerative diseases. The research is guided by the following hypotheses, which aim to contribute novel insights into the pathological mechanisms and diagnostic challenges associated with SD and SNAP.

1.2.1. Study 1: Differentiation of SD

The primary objective of this study is to examine the hypothesis that macrostructural and microstructural changes in brain regions, as assessed by volume and texture metrics, reveal distinct patterns among NC, AD, and SD. The secondary objective is to assess the impact of integrating volume and texture features on diagnostic accuracy for distinguishing SD from NC and AD, in comparison to single-modality models. The following sub-hypotheses have been postulated:

1) SD exhibits distinct structural atrophy, primarily in the anterior temporal lobe regions, that differentiates it from NC and AD.

2) Texture metrics, capturing microstructural alterations in key brain regions, reveal unique patterns in SD that further distinguish it from NC and AD.

3) A composite diagnostic model integrating volume and texture metrics will achieve superior performance in differentiating SD from NC and AD compared to models relying on single-modality features.

1.2.2. Study 2: Differentiation of SNAP

The primary objective of this study is to examine the hypothesis that macrostructural and microstructural changes, as measured by volume and texture metrics, can distinguish neurodegenerative patterns associated with NC, AD, and SNAP. The secondary objective is to assess the impact of integrating volume and texture features on diagnostic accuracy for distinguishing SNAP from NC and AD, in comparison to single-modality models. The following sub-hypotheses have been postulated:

1) SNAP exhibits distinct structural atrophy, particularly in the hippocampus and temporal lobe, that differentiates it from NC and AD.

2) Texture metrics, capturing microstructural alterations in key brain regions, reveal unique patterns in SNAP that further distinguish it from NC and AD.

3) A composite diagnostic model integrating volume and texture metrics will achieve superior performance in differentiating SNAP from NC and AD compared to models relying on single-modality features.

2. Methods

2.1. Study participants

This study employs a divided analytical approach, comparing NC, AD, and SD in Study 1 and NC, AD, and SNAP in Study 2, rather than analyzing all four groups simultaneously. This approach is predicated on the recognition that SD and SNAP exhibit distinct diagnostic processes and epidemiological and clinical characteristics.

While both conditions lack molecular imaging markers for definitive diagnosis, SD can be diagnosed by integrating clinical symptoms and structural brain imaging findings using the diagnostic criteria proposed by Neary et al. (David Neary et al., 1998),whereas SNAP is diagnosed based on exclusion criteria. Specifically, SNAP is identified when clinical symptoms resemble those of AD but amyloid PET confirms the absence of amyloid deposition, following the ATN framework proposed by the National Institute on Aging–Alzheimer's Association (NIA-AA) (Jack Jr et al., 2018b). This distinction underscores the reliance of SNAP on exclusionary diagnostic criteria, contingent on the absence of biomarkers, while SD is determined by established clinical and imaging criteria.

Beyond the diagnostic disparities, a notable distinction emerges in the prevalence and clinical manifestation of both conditions. SD is a rare disease, affecting 3–5 individuals per 100,000 (Coyle-Gilchrist et al., 2016) (Ratnavalli et

al., 2002), while SNAP is relatively common, present in up to 25% of patients diagnosed with AD (Vos et al., 2015). This discrepancy necessitates the execution of separate analyses, as the combination of SD and SNAP into a single study would limit the statistical power to validate findings for either condition. Furthermore, matching variables such as age, gender, education, and disease severity is critical for SD analyses due to the small sample size. However, the differences in age of onset and progression between SD and SNAP make matching these variables challenging. Typically, the onset of SD occurs in individuals between the ages of 50 and 60, progressing rapidly and displaying a broad spectrum of dementia severity (Jack Jr et al., 2016). In contrast, SNAP predominantly manifests in individuals in their late 70s and is generally characterized by a milder presentation (Dani et al., 2017). Consequently, separate analyses are necessary to ensure methodological rigor and valid comparisons.

2.1.1. Study 1

We enrolled 30 patients with SD who visited the dementia clinics of three national university hospitals (Seoul National University Bundang Hospital [SNUBH], Seoul Metropolitan Government–Seoul National University Boramae Medical Center [BMC], and Jeju National University Hospital [JNUH]). We enrolled 60 patients with AD from among the visitors to the dementia clinics of SNUBH whose age, sex and education level were matched to those of the 30 patients with SD. We enrolled 60 controls with NC whose age, sex, and education

level were matched to those of the 30 patients with SD from the Korean Longitudinal Study on Cognitive Aging and Dementia (KLOSCAD). The KLOSCAD is a nationwide population-based prospective cohort study of older Koreans. In the KLOSCAD, 6,818 community-dwelling Koreans aged ≥ 60 years were randomly sampled from 30 villages and towns across South Korea using residential rosters. The baseline evaluation was conducted in 2010–2012, and follow-up evaluations were conducted every 2 years until 2020. (Han et al., 2018)

2.1.2. Study 2

We recruited 502 community-dwelling older adults aged 60 years or older: 288 visitors to the Dementia Clinic at Seoul National University Bundang Hospital and 214 participants of the KLOSCAD who were enrolled at SNUBH. All participants were free of major psychiatric disorders (including mood disorder and substance use disorder), major neurological disorders (including movement disorder, epilepsy, and cerebrovascular disease), and other serious medical conditions that could affect cognition. The participants were confirmed to have no evidence of infarct, severe white matter hyperintensities (WMH), or hemorrhage on brain MRI. The absence of WMH was defined as a grade 2 or below on the Fazekas' scale on FLAIR brain MRI scans (Fazekas et al., 1987).

2.2. Research ethics

All participants were fully informed of the study protocol and provided written informed consent by themselves or their legal guardians. The study

205 protocol was approved by the Institutional Review Board of SNUBH (IRB No. B-
206 2005-615-001) and KLOSCAD (IRB No. B-0912-089-010).

207 2.3. Diagnostic assessment

208 Geriatric neuropsychiatrists administered standardized diagnostic
209 interviews that included medical history and physical and neurological
210 examinations according to the Korean version of the Consortium to Establish a
211 Registry for Alzheimer's Disease Assessment Packet Clinical Assessment Battery
212 (CERAD-K) (Lee et al., 2002) and the Korean version of the Mini International
213 Neuropsychiatric Interview. (Yoo et al., 2006) Research neuropsychologists or
214 trained nurses administered the CERAD-K Neuropsychological Assessment
215 Battery. (Lee et al., 2004) The CERAD-K Neuropsychological Assessment
216 Battery consists of nine neuropsychological tests: Verbal Fluency Test, Boston
217 Naming Test, Mini-Mental State Examination, Word List Memory Test, Word List
218 Recall Test, Word List Recognition Test, Constructional Praxis Test,
219 Constructional Recall Test, Trail Making Test A/B. (Lee et al., 2002)
220 A panel of geriatric psychiatrists then determined the final diagnosis and
221 Clinical Dementia Rating (CDR) (Morris, 1993) of the participants. We diagnosed
222 dementia and other major Axis I psychiatric disorders according to the diagnostic
223 criteria of the Diagnostic and Statistical Manual of Mental Disorders, Fourth
224 Edition (DSM-IV) (Bell, 1994) and mild cognitive impairment (MCI) according
225 to the consensus criteria of the International Working Group on MCI. (Winblad et

226 al., 2004)

227 The diagnoses of NC, AD, and SNAP followed the NIA-AA ATN
228 framework. In the current study, NC, AD, and SNAP were classified by Aβ
229 pathology (A) and neurodegeneration (N) because tau PET is not yet available in
230 Korea (Figure 1). Specifically, A represents aggregated amyloid-β or associated
231 pathological states, evaluated using cerebrospinal fluid (CSF) Aβ42 or
232 Aβ42/Aβ40 ratio and amyloid PET imaging. N indicates neurodegeneration or
233 neuronal injury, measured using structural MRI (e.g., medial temporal atrophy),
234 FDG PET hypometabolism, or CSF total tau levels. Using this framework,
235 participants were classified into three groups:

236 (1) Aβ-negative cognitively normal individuals without
237 neurodegeneration (NC; A-N-),

238 (2) Aβ-positive cognitively impaired individuals with neurodegeneration
239 (AD; A+N+), and

240 (3) Aβ-negative cognitively impaired individuals with neurodegeneration
241 (SNAP; A-N+).

242 In this study, the absence of amyloid beta deposition (A-) was defined as
243 a brain amyloid plaque load (BAPL) score of below grade 2 on a ^{18}F-florbetaben
244 PET scan (Barthel et al., 2011). The BAPL score was rated by neuroradiologists.
245 The presence of neurodegeneration (N+) was defined as grade 2 or higher medial
246 temporal atrophy (MTA) on coronal slices of T1-weighted brain MRI according to
247 the Scheltens scale (Scheltens et al., 1992). It is important to note that

248 pathological changes in SNAP may begin before clinical symptoms become
249 evident, as is the case in AD (Douglas & Scharre, 2019). Therefore, participants at
250 mild stages of disease were included in the present study.

251 The diagnosis of SD was made in accordance with the consensus clinical
252 diagnostic criteria proposed by Neary et al. (D. Neary et al., 1998), which define
253 semantic dementia as a subtype of frontotemporal lobar degeneration. The
254 aforementioned criteria emphasize a progressive deterioration of semantic
255 knowledge, characterized by impaired word comprehension (semantic aphasia)
256 and associative agnosia. Patients with SD frequently exhibit fluent but
257 meaningless speech, difficulty naming objects (anomia), and impaired
258 understanding of word meaning, while retaining relatively preserved episodic
259 memory and visuospatial skills in the early stages. To ensure diagnostic accuracy,
260 all SD cases from SNUBH, with the exception of those from external hospitals,
261 were confirmed as amyloid-negative using 18F-florbetaben PET imaging due to
262 the potential overlap with AD. Nevertheless, as comparable studies typically
263 adhere to diagnostic criteria without confirming amyloid negativity, this limitation
264 does not undermine the generalizability of the findings.

265 2. 4. MRI acquisition and preprocessing

266 Three-dimensional (3D) T1-weighted spoiled gradient-echo magnetic
267 resonance images in Digital Imaging and Communications in Medicine (DICOM)
268 format were acquired at SNUBH using a 3.0 T Achieva scanner (Philips Medical

Systems; Eindhoven, The Netherlands). The images were acquired using the following parameters: voxel size of 1.0 × 0.5 × 0.5 mm^3, 1.0 mm sagittal slice thickness with no inter-slice gap, echo time of 4.6 ms, repetition time of 8.1 ms, flip angle of 8° and a matrix size of 175 × 240 × 240 in the x, y, and z dimensions in SNUBH; voxel size of 1.0 × 1.0 × 1.0 mm^3, 1.0 mm sagittal slice thickness with no inter-slice gap, echo time of 4.6 ms, repetition time of 9.9 ms, flip angle of 8° and a matrix size of 180 × 220 × 200 in the x, y, and z dimensions in BMC; voxel size of 1.0 × 1.0 × 1.0 mm^3, 1.0 mm sagittal slice thickness with no inter-slice gap, echo time of 3.7 ms, repetition time of 8.2 ms, flip angle of 8° and a matrix size of 190 × 256 × 256 in the x, y, and z dimensions in JNUH. The original DICOM format images were converted to Neuroimaging Informatics Technology Initiative (NIfTI) format images and resliced into isovoxels of 1.0 × 1.0 × 1.0 mm^3. Whole-brain structures were then segmented into brain regions as defined by the Desikan-Killiany-Tourville (DKT) atlas using FreeSurfer version 6.0 (http://surfer.nmr.mgh.harvard.edu). (Fischl et al., 2002) The FreeSurfer recon-all process starts with motion correction, non-uniform intensity normalization, and skull stripping in the first step. In the second step, full-scale volumetric labelling and automatic topology fixing are performed. In the final step, spherical mapping and cortical parcellation are performed. After the recon-all process, we obtained parcellated individual brain masks of all regions of interest (ROIs) of the cerebrum according to the DKT atlas. (Klein & Tourville, 2012)

291 ## 2.5. Amyloid PET acquisition and preprocessing

292 The ^{18}F-florbetaben (FBB) PET images were acquired using a Discovery
293 VCT scanner (General Electric Medical Systems; Milwaukee, WI, USA). ^{18}F-
294 florbetaben (Neuraceq, Piramal, Mumbai, India) was injected slowly (6 s/mL)
295 with a total volume of up to 10 mL. After a 90-minute uptake period, PET images
296 were acquired for 20 minutes, consisting of four 5-minute dynamic frames. The
297 FBB PET images were processed using the PetSurfer procedure (FreeSurfer
298 version 6.0; http://surfer.nmr.mgh.harvard.edu/fswikiPetSurfer/) to perform co-
299 registration. The individual FBB PET was co-registered to the corresponding
300 native T1-weighted MRI using a rigid-body registration with mutual information
301 cost function. In addition, a 4 mm full width at half maximum (FWHM)
302 smoothing was applied in order to avoid the partial volume effect.

303 ## 2.6. Analysis of volume and texture of 3D T1-weighted MRI

304 We measured regional brain volume and total brain volume (TBV) using
305 FreeSurfer version 6.0 (http://surfer.nmr.mgh.harvard.edu). (Fischl et al., 2002)
306 We used TBV as the sum of the volumes of all structures identified in the
307 aseg.mgz file by the *recon-all* function in FreeSurfer.

308 Before calculating the regional brain textures, we performed an additional
309 pre-processing of the 3D T1-weighted brain MRI. For histogram normalization,
310 the partial volume effect was corrected by including voxels with intensity values
311 between [$\mu - 3\sigma$] and [$\mu + 3\sigma$] only (μ, mean; σ, standard deviation). (Collewet et

al., 2004) Then, the signal intensity of each grey matter voxel was normalized with respect to the participant's mean cerebrospinal fluid (CSF) signal intensity in the lateral ventricles to correct for inter-individual variation. Finally, the grey levels in each regional image were quantized by rescaling all signal intensity values to a uniform range of 32 to reduce discrete values, thereby avoiding statistical problems associated with sparse matrices in the computation of texture features. (Patel et al., 2008)

Subsequently, a 3D grey-level co-occurrence matrix (GLCM) was calculated in MATLAB R2021a (MathWorks, Natick, MA, USA) to extract texture features from each pre-processed regional image. The GLCM is an N × N matrix, where N represents the total number of grey levels present within the image. The matrix element (i,j) denotes the frequency of specific grey level pairs, including the reference voxel i and the neighboring voxel j, occurring at distance d and direction θ. 3D GLCMs were generated at a distance of d = 1 from each other (directly adjacent voxels) in 13 different directions. Based on the averaged 13 GLCMs, the "contrast" in each region was calculated using Haralick texture features (Haralick et al., 1973). The contrast texture feature measures local grey-level variation in an image, reflecting both the spatial distribution and the relative difference in gray- levels of adjacent voxels. Specifically, contrast increases as the difference in grey-levels between adjacent voxel pairs increase, enabling the simplest and most intuitive interpretation of texture changes. The formula for calculating contrast is shown below.

$$\text{Contrast} = \sum_{1=1}^{N}\sum_{j=1}^{N}(i-j)^2\ P_{i.j}$$

Where

N, the number of distinct gray levels in the quantized image

Pi,j, (i,j)th entry in a normalized gray-level co-occurrence matrix

Figure 2 illustrates examples of homogeneity and heterogeneity observed in MRI scans, along with the corresponding contrast scale. Homogeneous regions exhibit low contrast values, while heterogeneous regions display high contrast values, highlighting their role in capturing microstructural changes.

2.7. Statistical analysis

We compared demographic and clinical characteristics between groups using one-way analysis of variance (ANOVA) with Bonferroni post hoc comparison. We compared regional brain volumes between groups using one-way analysis of covariance (ANCOVA) adjusted for TBV and regional brain textures between groups using one-way ANCOVA adjusted for corresponding regional brain volumes with Bonferroni post hoc comparison.

We developed volume-based and texture-based models for classifying diagnostic groups using logistic regression with a forward selection of variables.

Furthermore, we proposed a composite model by combining the significant features from the volume-based and texture-based models. We estimated the classification performance of the models using receiver operator characteristic (ROC) curve analysis and compared the area under the ROC curve (AUC) between the models according to Hanley and McNeil. (Hanley & McNeil, 1983)

A two-tailed P value < 0.05 was considered statistically significant in all analyses. All statistical analyses were performed using the Statistical Package for the Social Sciences (SPSS) version 25.0 (IBM Corporation; Armonk, NY, USA) on Windows and MedCalc for Windows version 18.11.3 (MedCalc Software, Mariakerke, Belgium).

3. Results

This study investigated neurodegenerative patterns in SD and SNAP by comparing these groups with NC and AD. Using both volume and texture metrics, different patterns of degeneration were identified in SD and SNAP. Texture analysis provided additional insights beyond traditional volumetric measures, and composite models integrating volume and texture consistently showed superior diagnostic performance.

3.1. Study 1

Table 1 summarizes the demographic and clinical characteristics of the study participants, including NC, AD, and SD groups. Age, sex distribution, and education level did not significantly differ among the three groups. However, there were significant differences in total brain volume and cognitive performance as measured by the MMSE. The NC group demonstrated larger total brain volumes compared to both AD and SD groups ($p < 0.001$), suggesting greater brain atrophy in patient groups. Similarly, MMSE scores were significantly higher in the NC group compared to both AD and SD ($p < 0.001$), reflecting more severe cognitive impairment in these dementia groups.

Table 2 presents comparisons of regional brain volumes among NC, AD, and SD groups. Significant volume reductions were observed in both AD and SD patients compared to NC in key temporal lobe regions, including the amygdala, hippocampus, entorhinal cortex, parahippocampal gyrus, inferior temporal cortex, middle temporal cortex, and superior temporal cortex. In addition, SD patients demonstrated significantly smaller volumes in the entorhinal cortex, inferior temporal cortex, superior temporal cortex and temporal pole compared to AD. Frontal lobe regions such as the orbitofrontal cortex and frontal pole also showed significant volume reductions in SD patient groups compared to NC. These findings underscore distinct patterns of atrophy in SD and AD, particularly within the temporal lobe.

Texture analyses, summarized in Table 3, revealed significant differences in microstructural alteration across groups. Both AD and SD groups exhibited higher texture values compared to NC in multiple temporal lobe regions, including the entorhinal cortex, parahippocampal gyrus, fusiform gyrus, inferior temporal cortex, middle temporal cortex, superior temporal cortex, transverse temporal gyrus. In particular, SD patients demonstrated significantly higher texture values in the entorhinal cortex, inferior temporal cortex, middle temporal cortex, superior temporal cortex and temporal pole compared to AD, suggesting more pronounced microstructural alterations in these regions in SD. Conversely, AD patients showed higher texture values in the amygdala and hippocampus compared to SD, consistent with greater structural change in these regions in AD. Texture differences in frontal lobe regions were less pronounced but still significant in both patient groups compared to NC. Notably, SD exhibited greater changes in the frontal lobe regions, such as the frontal pole, compared to AD. Overall, these texture findings highlight unique microstructural characteristics that differentiate AD and SD.

The logistic regression models using volume and texture features successfully differentiated patients with SD from NC (Table 4). In the volume-based model, the entorhinal cortex and temporal pole showed significant contributions, with the entorhinal cortex demonstrating the strongest association (B = -2.029, p = 0.001, 95% CI = 0.042–0.417). In the texture-based model, the

entorhinal cortex (B = 1.773, $p < 0.001$, 95% CI = 0.240–15.488) and temporal pole (B = 1.309, p = 0.008, 95% CI = 1.405–9.762) were significantly associated with the classification. These findings suggest that both volume and texture features of these regions play important roles in distinguishing SD from NC.

The composite logistic regression model, combining volume and texture features, demonstrated additional insights for differentiating NC from SD (Table 5). Among the features, the texture of the entorhinal cortex was a significant predictor (B = 1.018, p = 0.048, OR = 2.766, 95% CI = 1.007–7.600). Although the volume of the entorhinal cortex showed a trend towards significance (B = -1.393, p = 0.061, OR = 0.248, 95% CI = 0.058–1.069), its predictive power was less pronounced compared to the texture feature. These results highlight the complementary roles of volume and texture in identifying SD.

The performance metrics of the volume-based, texture-based, and composite models in classifying NC from SD are summarized in Table 6. The composite model achieved the highest AUC (0.983), with excellent sensitivity (86.7%), specificity (98.3%), PPV (96.3%), and NPV (93.7%). The texture-based model also performed well, with an AUC of 0.966, sensitivity of 86.7%, perfect specificity (100.0%), PPV (100.0%), and NPV (93.8%). The volume-based model showed slightly lower performance compared to the composite model, with an AUC of 0.963, sensitivity of 80.0%, specificity of 95.0%, PPV of 88.9%, and NPV of 90.5%. These results suggest the enhanced discriminative ability of the

composite model by integrating both volume and texture features. However, pairwise comparisons of AUC values using the Hanley and McNeil method revealed p-values of 0.516 for the volume-based model versus the composite model and 0.557 for the texture-based model versus the composite model, indicating that the performance differences between the models were not statistically significant.

The logistic regression models for differentiating SD from AD identified key regional predictors in both volume and texture features (Table 7). In the volume-based model, the hippocampus (B = 0.602, p = 0.007, 95% CI = 1.178−2.827) and the temporal pole (B = -1.603, p < 0.001, 95% CI = 0.209–0.570) were significant predictors. Similarly, in the texture-based model, the hippocampus (B = -0.618, p = 0.005, 95% CI = 0.349–0.833) and the temporal pole (B = 0.982, p < 0.001, 95% CI = 1.595–4.470) were significant contributors. These findings emphasize the importance of both hippocampal and temporal pole features in distinguishing SD from AD.

The composite logistic regression model combining volume and texture features enhanced the ability to differentiate SD from AD (Table 8). The temporal pole volume (B = -0.834, p = 0.003, OR = 0.434, 95% CI = 0.252–0.749) and hippocampal texture (B = -0.529, p = 0.033, OR = 0.589, 95% CI = 0.362–0.959) were significant predictors, with the temporal pole texture also showing strong associations (B = 0.718, p = 0.011, OR = 2.050, 95% CI = 1.180–3.561).

The performance metrics of the volume-based, texture-based, and

composite models in classifying Alzheimer's disease from semantic dementia are summarized in Table 9. The composite model achieved the highest AUC (0.862), with sensitivity of 66.7%, specificity of 91.7%, PPV of 80.0%, and NPV of 84.6%. The texture-based model demonstrated an AUC of 0.816, sensitivity of 53.3%, specificity of 91.7%, PPV of 76.2%, and NPV of 79.7%. The volume-based model showed the lowest performance, with an AUC of 0.806, sensitivity of 56.7%, specificity of 88.3%, PPV of 70.8%, and NPV of 80.3%. These results underscore the enhanced discriminative ability of the composite model by integrating both volume and texture features. However, pairwise comparisons of AUC values using the Hanley and McNeil method revealed p-values of 0.418 for the volume-based model versus the composite model and 0.500 for the texture-based model versus the composite model, indicating that the performance differences between the models were not statistically significant. Overall, these findings emphasize the distinct structural and microstructural differences in the temporal pole and hippocampus between SD and AD, highlighting the critical role of microstructural changes in the temporal regions for distinguishing SD.

3.2. Study 2

Table 10 summarizes the demographic and clinical characteristics of the participants across the three diagnostic groups: NC, AD, and SNAP. There were no statistically significant differences among the groups in age, sex, education level, or total brain volume. However, the MMSE scores differed significantly across

groups ($p < 0.001$). Post-hoc analyses revealed that the NC group scored significantly higher on the MMSE compared to both AD and SNAP groups, indicating more severe cognitive impairment in the patient groups. The NC group had an average MMSE score of 27.6, while the AD and SNAP groups scored 23.7 and 24.1, respectively.

Table 11 outlines the regional volume comparisons across diagnostic groups. Both the AD and SNAP groups demonstrated smaller volumes in key temporal lobe structures, including the amygdala, hippocampus, entorhinal cortex, inferior temporal cortex and middle temporal cortex compared to NC group. Parietal regions, such as the precuneus, also exhibited significant volume reductions in the AD group compared to NC.

As detailed in Table 12, significant differences in regional texture features were observed across diagnostic groups. Both AD and SNAP groups exhibited elevated texture heterogeneity in the temporal lobe, particularly in the amygdala, hippocampus, entorhinal cortex, parahippocampal gyrus, bankssts, inferior temporal cortex, middle temporal cortx and superior temporal cortex. In the frontal lobe, regions such as the inferior frontal cortex, middle frontal cortex and superior frontal cortex showed increased texture values in both patient groups, highlighting widespread microstructural changes extending beyond the temporal lobe. In the parietal lobe, AD exhibited subtle changes over a broader range, including regions where volume changes were more pronounced. Texture

differences in subcortical structures, such as the accumbens area, caudate, putamen and thalamus were also observed, with higher values in SNAP compared to NC. Interestingly, the thalamus exhibited significantly higher texture features in SNAP compared to both NC and AD, suggesting a distinct structural abnormality in this region.

Table 13 presents the logistic regression model parameters for differentiating participants with suspected non-Alzheimer's disease pathophysiology (SNAP) from normal controls (NC). In the volume-based model, hippocampal volume (B = -1.212, $p < 0.001$, 95% CI = 0.222–0.399) and middle temporal cortex volume (B = -0.403, $p = 0.014$, 95% CI = 0.484–0.923) were identified as significant predictors, showing reduced volumes in SNAP compared to NC. The texture-based model highlighted microstructural changes, with significant predictors including the amygdala (B = 0.818, $p < 0.001$, 95% CI = 1.688–3.041), entorhinal cortex (B = 0.797, $p < 0.001$, 95% CI = 1.681–2.932), superior frontal cortex (B = 1.327, $p < 0.001$, 95% CI = 2.396–5.929), posterior cingulate cortex (B = 0.345, $p = 0.017$, 95% CI = 1.063–1.875), and putamen (B = 0.564, $p < 0.001$, 95% CI = 1.425–1.763).

The composite logistic regression model for differentiating NC from SNAP is detailed in Table 14. The model revealed hippocampal volume as the strongest discriminator, with significant reductions observed in SNAP compared to NC (B = -0.910, $p < 0.001$, OR = 0.402, 95% CI = 0.289–0.560). Among

texture features, significant predictors included the amygdala (B = 0.366, p = 0.037, OR = 1.441, 95% CI = 1.023–2.031), entorhinal cortex (B = 0.401, p = 0.014, OR = 1.493, 95% CI = 1.085–2.055), and superior frontal cortex (B = 1.191, p < 0.001, OR = 3.291, 95% CI = 2.047–5.291).

The performance metrics of the volume-based, texture-based, and composite models in classifying SNAP from NC are summarized in Table 15. The composite model achieved the highest AUC (0.860), with sensitivity of 70.3%, specificity of 85.2%, PPV of 80.1%, and NPV of 77.2%. The texture-based model performed well, with an AUC of 0.838, sensitivity of 69.0%, specificity of 81.4%, PPV of 75.9%, and NPV of 75.6%. The volume-based model showed the lowest performance, with an AUC of 0.778, sensitivity of 64.5%, specificity of 78.7%, PPV of 71.9%, and NPV of 72.4%. Pairwise comparisons of AUC values using the Hanley and McNeil method showed that the composite model had a significantly higher AUC compared to the volume-based model (p = 0.014), while no significant difference was observed between the composite and texture-based models (p = 0.487).

Table 16 presents the logistic regression model parameters for differentiating participants with SNAP from those with AD. In the volume-based model, entorhinal cortex volume was a significant predictor (B = 0.178, p = 0.047, 95% CI = 1.002–1.425). The texture-based model identified additional predictors, including the superior temporal cortex (B = -0.454, p = 0.018, 95% CI = 0.437–

0.924), superior frontal cortex (B = 0.582, p < 0.001, 95% CI = 1.323–2.421), superior parietal cortex (B = -0.406, p = 0.004, 95% CI = 0.507–0.876), and thalamus (B = 0.360, p = 0.002, 95% CI = 1.144–1.796). These findings highlight the contribution of both temporal and parietal regions, as well as subcortical structures, in differentiating SNAP from AD.

The composite model parameters for differentiating AD from SNAP are provided in Table 17. The model showed significant associations for texture-based features, including the superior temporal cortex (B = -0.391, p = 0.047, OR = 0.676, 95% CI = 0.460–0.998), superior frontal cortex (B = 0.568, p < 0.001, OR = 1.765, 95% CI = 1.305–2.387), superior parietal cortex (B = -0.428, p = 0.002, OR = 0.652, 95% CI = 0.494–0.859), and thalamus (B = 0.361, p = 0.002, OR = 1.435, 95% CI = 1.125–1.798). These results suggest that microstructural changes in parietal and subcortical regions play a critical role in differentiating AD from SNAP, while volume-based features such as the entorhinal cortex volume were not significant in the composite model.

The performance metrics for classifying AD and SNAP using volume, texture, and composite models are summarized in Table 18. The composite model achieved the highest AUC (0.699), with sensitivity of 63.2%, specificity of 67.1%, PPV of 64.5%, and NPV of 65.9%. The texture-based model followed, with an AUC of 0.693, sensitivity of 63.2%, specificity of 65.9%, PPV of 63.6%, and NPV of 65.5%. The volume-based model showed the lowest performance,

with an AUC of 0.567, sensitivity of 45.8%, specificity of 67.1%, PPV of 56.8%, and NPV of 56.7%. Pairwise comparisons of AUC values using the Hanley and McNeil method showed that the composite model had a significantly higher AUC compared to the volume-based model ($p = 0.002$), while no significant difference was observed between the composite and texture-based models ($p = 0.880$). These findings suggest that texture features contribute more to the classification of AD and SNAP compared to volume features, and the composite model provides marginal improvements in performance.

4. Discussions

Overview of Findings

This study investigated the unique neurodegenerative patterns in diseases that share similarities with AD, specifically SD and SNAP, using MRI-based volume and texture analysis. SD showed focal atrophy and textural changes localized to the anterior temporal lobe, reflecting selective degeneration in semantic processing circuits. Meanwhile, SNAP demonstrated non-amyloid neurodegeneration characterized by focal atrophy and texture changes, including microstructural alterations in the subcortical areas.

Composite models integrating volume and texture consistently

outperformed single-modality models in diagnostic accuracy, providing the most robust and accurate tools for distinguishing between SD, SNAP, and AD. These results underline the importance of integrating volume and texture metrics to enhance differential diagnosis and deepen our understanding of the pathophysiological differences between neurodegenerative diseases.

Semantic Dementia and Alzheimer's Disease

SD and AD share certain commonalities, including atrophy in the temporal lobe. (Basso et al., 2006) (Teipel et al., 2006) (Tomé et al., 2023) However, the results of this study demonstrate that SD exhibits a distinct pattern of neurodegeneration, particularly in the anterior temporal pole and associated regions, which are not typically affected in AD. Texture analysis revealed significant alterations in the temporal pole in SD compared to AD, capturing early microstructural disorganization linked to tau or TDP-43 pathology.

Both SD and AD groups showed smaller volumes across all ROIs in both hemispheres compared to NC, but SD demonstrated significantly smaller volumes in key temporal regions, including the entorhinal cortex, inferior temporal cortex, superior temporal cortex, and temporal pole. These structural differences were further complemented by texture findings, as SD showed elevated texture values in these regions, indicating pronounced microstructural alterations. In AD, atrophy appears to start in the hippocampus and gradually spread to other temporal structures as the disease progress. In contrast, in SD, cortical atrophy is most

prominent in temporal poles, where atrophy does not usually occur in normal aging. (Collins et al., 2017; Rogalski et al., 2014; Scahill et al., 2002)

Figure 2 provides a three-dimensional visualization of volume and texture changes in AD and SD groups, showing both lateral and medial views. In the SD group, significant volume reductions and texture changes were observed in the temporal pole and parts of the frontal lobe, reflecting the focal atrophy characteristic of semantic dementia. In contrast, AD exhibited more diffuse changes in medial temporal regions, such as the hippocampus and amygdala, where pronounced volume loss and texture abnormalities were identified. In summary, atrophy in AD was most prominent in the hippocampus and amygdala, with texture changes extending beyond these structures to surface regions, indicating a medial-to-lateral progression. However, in SD, marked atrophy and texture changes were observed in the temporal lobe, with alterations spreading from the temporal pole to other regions, suggesting an anterior-to-posterior progression.

Figure 3 illustrates the performance of volume-based, texture-based, and composite models for differentiating SD from NC and AD. The composite model consistently achieved the highest AUC for both NC vs. SD (0.983) and AD vs. SD (0.862) classifications, demonstrating the complementary value of integrating texture and volume features. Texture-based models outperformed volume-based models in both comparisons, highlighting the sensitivity of texture analysis to subtle microstructural changes.

621 The MMSE, a global cognitive assessment, showed similar scores between
622 AD and SD patients, but differences were observed in specific cognitive domains
623 (Supplementary table 1). SD patients demonstrated significantly lower scores in
624 language-related tasks, such as VFT and BNT, compared to AD patients, indicating
625 more severe deficits in language functions. To examine the association between
626 cognitive performance and regional volume and texture in SD, we performed
627 Pearson correlation analysis. (Supplementary table 2 and table 3). Certain regional
628 volumes showed strong correlations with VFT, BNT, and DST tasks. Examining the
629 influence of verbal fluency, naming tests, and the digit span, which measures verbal
630 short-term memory, highlights the pronounced language-related deficits in SD.
631 Similarly, regional texture also demonstrated correlations with VFT, BNT, DST, as
632 well as TMT-A. Considering the association with TMT-A, which is related to
633 executive function, the findings suggest the presence of executive function
634 impairments in SD. Longitudinal analyses would be valuable for tracking the
635 detailed cognitive impacts over time.

636 Suspected Non-Alzheimer's Disease Pathophysiology and 637 Alzheimer's Disease

638 Our study reveals that texture analysis of brain MRI is more effective than
639 traditional volumetric measures in detecting early neurodegenerative changes in
640 SNAP. Significant textural differences in multiple brain regions indicate that
641 microstructural alterations precede volumetric loss and cognitive impairment.

Texture analysis revealed significant microstructural changes in the subcortical regions in SNAP, which were less pronounced in AD. These differences suggest distinct underlying mechanisms, such as TDP-43 or alpha-synuclein pathology, contributing to SNAP's neurodegenerative trajectory. (Wisse et al., 2021) (Vos et al., 2024) Although hippocampal atrophy has been consistently reported in both AD and SNAP, (Burnham et al., 2016; Chung et al., 2017; Gordon et al., 2016) (Vijayakumar & Vijayakumar, 2013) Texture analysis in this study revealed that microstructural changes extend to non-traditional regions, with alterations in the thalamus being particularly discriminative for SNAP. This emphasizes the sensitivity of texture metrics in capturing early neurodegeneration, aligning with previous studies demonstrating the ability of MRI texture to detect subtle tissue changes indicative of early neurodegenerative processes. (Kwon et al., 2023; Lee et al., 2020)

The present study revealed that texture differences in the parietal lobe were relatively minor between the control group and the SNAP group, whereas previous neuroimaging studies on AD have consistently reported significant atrophy in this region. (Pyun et al., 2017; Scahill et al., 2002) For instance, volumetric analyses have demonstrated reductions in grey matter volume in the parietal lobule and cingulate regions in AD patients, with extensive atrophy also observed in regions such as the precuneus, superior parietal cortex, inferior parietal cortex, and supramarginal gyrus as the disease progresses to dementia. (Guo et al., 2010) While

AD exhibited significant texture alterations in the parietal regions, SNAP showed elevated texture values in subcortical areas such as the thalamus. These findings suggest that SNAP may involve distinct neurodegenerative mechanisms, potentially driven by non-amyloid pathologies like TDP-43 or alpha-synuclein, which differ from the amyloid-driven pathology in AD. Despite the shared neurodegeneration in the temporal lobe, the differentiation between SNAP and AD becomes clearer when considering other brain regions. This supports the hypothesis that SNAP follows a unique pathological trajectory or resilience mechanisms not observed in AD. (Pyun et al., 2017)

Figure 4 further elucidates regional volume and texture changes in AD and SNAP. While volume reductions in SNAP are less pronounced compared to AD, particularly in the hippocampus and temporal lobe regions, significant texture alterations are evident in the subcortical areas, such as the thalamus. This suggests that SNAP involves unique microstructural changes compared to AD, which may reflect distinct underlying neurodegenerative mechanisms. These observations highlight the potential of texture analysis as a sensitive tool for identifying and tracking neurodegenerative processes in SNAP.

Figure 5 highlights the performance of volume-based, texture-based, and composite models for classifying SNAP. The composite model consistently achieved the highest AUC for both NC vs. SNAP (0.860) and AD vs. SNAP (0.699) comparisons. These findings underscore the sensitivity of texture analysis in

capturing early microstructural changes in SNAP and the value of combining texture and volume features. Future studies should explore the integration of texture metrics with biomarkers to improve the stratification of SNAP subtypes.

The cognitive test performance by diagnostic groups is summarized in Supplementary table 4. Most cognitive domains show similar performance between the AD and SNAP groups, but the AD group demonstrates more severe deficits in memory-related tasks, such as WLRT. Volume features of SNAP, particularly regional volumes in the temporal lobe, strongly correlate with language, memory, and executive function tasks (Supplementary table 5). However, texture features exhibit weaker correlations compared to volume features (Supplementary table 6). This may be attributed to the pathological heterogeneity of SNAP and the subtle changes characterizing its early stages. Additionally, texture alterations in specific regions may not adequately explain associations with cognitive performance, potentially due to the mild state of patients within the SNAP group. Furthermore, while texture analysis effectively captures microstructural changes, it may not consistently influence all cognitive domains, resulting in limited correlations. Moreover, the heterogeneity of the disease makes it difficult to identify specific patterns of cognitive impairment. Future longitudinal studies should aim to clarify the temporal relationship between texture alterations and cognitive decline in SNAP.

Implications of the Study

This study highlights the complementary roles of volume and texture

analysis in differentiating SD and SNAP from AD and NC. Volume reflects macroscopic structural changes due to neuronal loss and atrophy, while texture is sensitive to subtle microstructural changes that may occur earlier in disease progression. The combination of these metrics improves diagnostic accuracy by capturing changes that volume alone may miss, particularly in diseases like SNAP where atrophy is less pronounced. In clinical practice, MRI-based volume and texture analysis can serve as a valuable tool for diagnosing SD and SNAP. For SD, texture abnormalities in regions such as the entorhinal cortex and temporal pole align with its known pathology. For SNAP, texture analysis provides a non-invasive way to identify subtle changes in the brain, which is particularly useful when amyloid PET imaging is unavailable or not feasible. This approach reduces reliance on costly or invasive biomarker assessments, making MRI a practical alternative. Specifically, texture analysis contributes to the clinical diagnostic process by aiding early prediction and classification, particularly in initial stages where volume-based methods may face limitations. For instance, texture analysis may improve the early detection of subtle microstructural changes that traditional approaches might overlook. While its contribution might be limited in mild conditions like SNAP, texture metrics could offer greater utility in rapidly progressing diseases such as SD, providing valuable diagnostic insights. The findings also emphasize the clinical implications of distinguishing SD and SNAP. In early stages, texture analysis may help identify these conditions more accurately, guiding appropriate diagnostic and treatment strategies. Additionally, recognizing SNAP's slower progression and

mild clinical symptoms highlights the need for non-invasive tools like MRI to assist in its identification.

Broader Implications of Texture Analysis

MRI texture has been shown to correlate with radiographic pathologies validating its utility as an indicator of early neurodegenerative changes. (Lee et al., 2021) For example, texture features in the medial pulvinar have been found to distinguish dementia with Lewy bodies (DLB) from control groups, despite comparable volumes, underscoring the broader applicability of texture analysis across diverse neurodegenerative diseases. (Tak et al., 2020) These findings highlight that subtle microstructural changes, such as variations in neuronal density, myelin, and tissue integrity, may be detectable before volumetric loss and cognitive impairment. (Zhang et al., 2013)

The ability of texture analysis to reveal microstructural alterations in subcortical and cortical regions underscores its potential as a broadly applicable neuroimaging tool. For instance, the elevated texture heterogeneity observed in the thalamus in SNAP, and in the temporal pole in SD, highlights its utility in capturing pathology-specific patterns across neurodegenerative diseases. These findings suggest that texture metrics could complement existing biomarkers, particularly in the early and differential diagnosis of conditions such as SNAP and SD, where traditional volumetric measures may be insufficient. Furthermore, recent studies suggest that TDP-43 pathology interacts with tau aggregation, exacerbating

748 neurofibrillary tangle formation (Tomé et al., 2023). This interaction underscores
749 the potential for texture analysis to detect early microstructural changes driven by
750 synergistic pathologies. Future work should prioritize integrating texture metrics
751 with pathological and molecular markers for a more comprehensive understanding
752 of disease mechanisms. Specifically, future studies should examine the associations
753 between tau PET imaging, myelin content, and texture metrics to elucidate their
754 potential relationships. This could reveal how texture analysis serves not only as a
755 complementary tool to volumetric measures but also as a potential link to
756 pathological markers, providing deeper insights into disease processes.

757 SNAP is a heterogeneous condition linked to various non-Aβ pathologies,
758 such as α-synucleinopathy, tau, and TDP-43 proteinopathy, which are associated
759 with non-AD dementias. (Wisse et al., 2021) (Vos et al., 2024) For instance, α-
760 synuclein pathology is present in dementia with Lewy bodies and Parkinson's
761 disease dementia, with observations of the pathology in the putamen, frontal, and
762 temporal regions. (Borghammer et al., 2010; Burton et al., 2002; Camicioli et al.,
763 2009; Cousins et al., 2003; Reetz et al., 2009; Seidel et al., 2017) Tau or TDP-43
764 each are responsible for approximately 50% of frontotemporal dementia cases. Tau
765 pathology is observed in the frontal lobe and thalamus, while TDP-43 is found in
766 the frontal and temporal cortex and hippocampus. (Cairns et al., 2007; Davidson et
767 al., 2007; Rohrer & Rosen, 2013) TDP-43 is also identified in ALS, affecting
768 similar brain regions. (Geser et al., 2009; Leigh et al., 1991; Neumann et al., 2006)

These findings suggest that texture may serve as an early neuroimaging marker for non-AD, offering a more sensitive metric for differentiating it from age-related cognitive decline and AD.

Clinical Implications of Early Disease Classification Using MRI

The capacity to differentiate between SNAP and SD through MRI-based volume and texture analysis holds significant clinical implications for diagnosis, prognosis, and treatment. Primarily, distinguishing between these conditions at early stages reduces reliance on invasive and costly diagnostic procedures, such as amyloid PET imaging. This streamlines the diagnostic process, enhances clinical workflow efficiency, and ensures broader accessibility for patients. Secondly, identifying distinct neurodegenerative patterns facilitates tailored predictions of disease progression. For instance, SNAP typically manifests with a more gradual progression and less severe symptoms compared to SD, which is marked by a rapid decline in cognitive abilities. The ability to distinguish between these conditions enables clinicians to provide precise prognostic information, helping patients and caregivers prepare for potential outcomes and necessary interventions. Lastly, precise differentiation informs targeted therapeutic strategies. Specifically, SD patients may benefit from interventions targeting deficits in semantic processing and language function, while SNAP patients require treatments that focus on non-amyloid pathologies, such as TDP-43 or tau-related mechanisms. Furthermore, early diagnosis facilitates the identification of candidates suitable for emerging

therapies targeting specific pathological substrates. This early classification framework ensures optimized patient management and supports the development of personalized treatment approaches.

Limitations and Future Directions

This study offers significant insights into neurodegenerative conditions; however, several limitations must be addressed to contextualize the findings. First, the cross-sectional design limits the ability to determine the temporal relationship between texture changes, volume loss, and cognitive decline. Longitudinal studies are necessary to evaluate whether texture changes precede volume alterations, offering deeper insights into disease progression and early diagnostic markers. Secondly, the lack of histopathological data hinders the establishment of direct correlations between texture alterations and specific pathological markers, such as tau or TDP-43, which would offer stronger biological validation for the observed imaging features. Thirdly, the study's capacity to perform internal and external validation was constrained due to the limited sample sizes. The rarity of SD (3–5 individuals per 100,000) resulted in a small sample size, precluding both internal and external validation. For SNAP, while the sample size allowed for internal validation, these results were not presented in the main analysis to maintain methodological consistency between Study 1 and Study 2. External validation for SNAP, as well as for SD, remains necessary and should be a focus of future research.

Additionally, the study did not consider potential confounding variables, such as lifestyle factors (e.g., diet, exercise, and smoking), or the impact of concurrent neurological or psychiatric conditions (e.g., depression or anxiety), which could influence brain structure and texture metrics. Incorporating these variables in future analyses would strengthen the generalizability and accuracy of findings. Furthermore, the reliance on a single imaging modality, although enhanced with texture and volume analyses, may have limited the ability to capture complex interactions between structural, functional, and molecular changes. Integrating multimodal imaging, such as fMRI, PET, or diffusion-weighted imaging, could provide a more comprehensive understanding of the disease mechanisms. Additionally, the lack of stratification based on disease subtypes or progression stages may have obscured specific trends or correlations unique to particular patient groups. Tailored subgroup analyses could provide more targeted insights into disease pathophysiology.

Finally, differences in MRI acquisition protocols, scanner hardware, and processing pipelines across sites may introduce variability, suggesting the need for standardized imaging procedures in multicenter studies. This variability underscores the importance of developing robust harmonization techniques or statistical adjustments to minimize inter-site differences.

To address these limitations, future research should explore enhancing the robustness of diagnostic models. One approach could be utilizing multicenter

datasets to enable external validation, particularly for rare conditions like SD. Expanding the integration of multimodal imaging techniques, such as diffusion-weighted imaging and molecular imaging, would provide a more comprehensive view of the microstructural changes underlying neurodegeneration. The development of machine-learning classifiers that incorporate texture and volume metrics, while accounting for variability in clinical presentations, has the potential to yield more accurate and reliable diagnostic tools. Additionally, incorporating advanced statistical techniques, such as latent class analysis or mediation modeling, could help identify hidden patterns or mechanisms underlying neurodegenerative processes. Longitudinal studies will also be crucial for assessing the clinical progression of these imaging changes and their temporal association with cognitive decline. Furthermore, combining texture analysis with biomarkers, such as fluid-based or genetic markers, will provide a more holistic approach to diagnosis and disease monitoring.

5. Conclusions

This study highlights the value of combining texture and volume analysis in exploring neurodegenerative diseases that mimic AD, such as SD and SNAP. While volume analysis captures macroscopic structural changes due to neuronal loss and atrophy, texture analysis detects early microstructural changes in key brain regions, offering complementary insights into the distinct pathological mechanisms

853 underlying these conditions. By integrating these approaches, it becomes possible
854 to improve early diagnosis, enable more accurate differentiation of non-AD
855 conditions from AD, and inform targeted therapeutic strategies. As such, the
856 combined use of texture and volume analysis represents a critical advancement in
857 the neuroimaging of dementia and other neurodegenerative diseases.

Table 1. Demographic and clinical characteristics between normal controls and patients with Alzheimer's disease and semantic dementia

	NC [a]	AD [b]	SD [c]	Statistics*	
	(n = 60)	(n = 60)	(n = 30)	*p*	Post-hoc
Age, years, mean (SD)	73.1 (6.0)	75.0 (7.5)	71.5 (8.3)	0.084	-
Sex, female, %	55.0	70.0	50.0	0.114	-
Education, years, mean (SD)	12.9 (4.0)	11.6 (4.9)	12.5 (5.4)	0.349	-
Total brain volume†, cc, mean (SD)	1009.8 (100.7)	935.7 (80.1)	961.2 (112.1)	<0.001	a > b
MMSE, points, mean (SD)	28.1 (1.8)	19.5 (5.3)	19.3 (5.2)	<0.001	a > b, c

AD, Alzheimer's disease; SD, semantic dementia; MMSE, Mini Mental State Examination;

†Sum of the volume of the structures identified in the Freesurfer aseg.mgz volume

*One-way analysis of variance for continuous variables and chi-square test for categorical variables with Bonferroni post hoc comparisons

Table 2. Comparison of regional volumes between normal controls and patients with Alzheimer's disease and semantic dementia

	NC [a]	AD [b]	SD [c]	Statistics*		
	(n = 60)	(n = 60)	(n = 30)	NC-AD	NC-SD	AD-SD
Temporal Lobe						
Amygdala	2740.5 (383.6)	2111.7 (346.4)	1979.2 (510.0)	**<0.001**	**<0.001**	**0.017**
Hippocampus	7220.4 (625.8)	5786.6 (715.3)	6170.8 (1329.1)	**<0.001**	**<0.001**	0.196
Entorhinal cortex	3895.5 (605.1)	2820.7 (605.7)	2467.3 (697.7)	**<0.001**	**<0.001**	**0.006**
Para hippocampal	3392.3 (420.2)	2942.8 (451.4)	2836.6 (518.3)	**<0.001**	**<0.001**	0.186
Fusiform	16461.8 (1709.4)	14682.9 (1897.4)	13981.5 (2143.9)	**<0.001**	**<0.001**	0.104
Bankssts	3872.9 (477.5)	3518.4 (432.0)	3534.7 (627.0)	**0.018**	**0.042**	0.704
Inferior temporal	19869.0 (2883.7)	16866.0 (2510.3)	15270.8 (3215.0)	**<0.001**	**<0.001**	**0.001**
Middle temporal	20188.8 (2390.9)	17418.7 (2445.9)	15925.3 (2994.3)	**<0.001**	**<0.001**	**0.002**
Superior temporal	20925.8 (2492.2)	18651.4 (1920.5)	17567.9 (2757.0)	**0.001**	**<0.001**	**0.002**
Transverse temporal	1759.5 (323.4)	1658.0 (268.2)	1655.6 (334.2)	0.447	0.237	0.594
Temporal pole	4840.8 (610.4)	4348.1 (690.7)	3520.5 (907.4)	0.100	**<0.001**	**<0.001**
Frontal Lobe						
Orbitofrontal	22511.1 (2334.2)	20893.8 (1988.3)	19549.8 (3207.0)	0.102	**<0.001**	**<0.001**
Inferior frontal	18451.2 (2094.3)	17014.2 (1763.3)	17191 (2053.9)	0.305	0.304	0.862
Middle frontal	36210.0 (4395.7)	33362.0 (3595.1)	34505.8 (5490.0)	0.309	0.412	0.657
Superior frontal	37387.4 (4134.0)	34589.5 (3588.5)	34442.3 (4793.9)	0.305	0.203	0.239
Precentral	24927.9 (2483.0)	24316.6 (1941.1)	24358.7 (2690.6)	0.795	0.761	0.523
Paracentral	6908.9 (877.7)	6699.3 (715.8)	6808.8 (763.3)	0.790	0.859	0.890
Frontal pole	1906.7 (219.7)	1837.3 (245.3)	1723.7 (248.6)	0.155	**0.001**	**0.030**

Anterior cingulate	7032.9 (984.9)	6618.1 (993.2)	6324.2 (1245.3)	0.596	0.109	0.403
Parietal Lobe						
Inferior parietal	23182.5 (2995.2)	21349.6 (2257.2)	21822.6 (3201.2)	**0.010**	0.141	0.948
Superior parietal	23103.6 (2272.2)	21552.8 (2109.3)	22311.7 (3012.2)	**0.024**	0.491	0.397
Postcentral	16471.1 (2049.9)	16333.9 (1912.6)	16807.1 (2287.9)	0.254	0.114	0.722
Precuneus	17276.2 (2108.1)	15690.7 (1707.7)	16152.9 (2637.8)	0.072	0.288	0.718
Supra marginal	18742.1 (2556.3)	17185.8 (2082.1)	17348.5 (2461.6)	0.018	0.054	0.741
Isthmus cingulate	4471.0 (609.7)	4055.0 (517.2)	4162.2 (792.4)	0.119	0.229	0.745
Posterior cingulate	5687.9 (710.8)	5169.5 (791.4)	5240.7 (945.4)	**0.038**	0.056	0.874
Occipital Lobe						
Cuneus	5305.2 (926.1)	5153.6 (573.6)	5482.2 (795.9)	0.500	0.106	0.061
Lingual	11205.5 (1449.5)	10822.5 (1409.0)	10982 (1561.0)	0.990	0.827	0.975
Lateral occipital	20417.7 (2982.2)	18907.9 (2310.2)	20019.4 (2705.7)	0.198	0.954	0.117
Pericalcarine	3726.3 (721.8)	3851.0 (668.3)	3858.9 (551.4)	0.074	0.217	0.895
Subcortical Regions						
Accumbens area	862.3 (159.0)	793.7 (116.4)	783.9 (183.6)	0.197	0.103	0.548
Caudate	6448.3 (899.6)	6298.7 (885.8)	6198.2 (938.4)	0.679	0.648	0.325
Putamen	8314.0 (993.3)	7873.0 (1004.9)	7649 (1085.8)	0.739	0.023	0.113
Pallidum	3342.9 (391.0)	3203.7 (481.0)	3279.6 (437.2)	0.961	0.943	0.965
Thalamus	11980.9 (1283.8)	11256.7 (1028.9)	11910.4 (1965.1)	0.130	0.365	0.083

Note. All values are presented as mean (standard deviation) in mm^3.

AD, Alzheimer's disease; SD, semantic dementia

*One-way analysis of covariance adjusting for total brain volume with Bonferroni post hoc comparisons

Table 3. Comparison of regional textures between normal controls and patients with Alzheimer's disease and semantic dementia

	NC [a] (n = 60)	AD [b] (n = 60)	SD [c] (n = 30)	Statistics*		
				NC-AD	NC-SD	AD-SD
Temporal Lobe						
Amygdala	22.6 (2.3)	24.6 (2.2)	23.2 (3.4)	**0.021**	0.065	**0.003**
Hippocampus	26.5 (2.1)	27.6 (2.2)	26.1 (3.3)	**0.020**	0.147	**0.009**
Entorhinal cortex	24.2 (2.3)	29.6 (3.6)	32.6 (4.9)	**<0.001**	**<0.001**	**0.031**
Para hippocampal	25.2 (2.2)	29.0 (3.5)	29.7 (4.1)	**<0.001**	**<0.001**	0.951
Fusiform	21.1 (2.4)	24.4 (2.2)	24.6 (2.8)	**<0.001**	**0.002**	0.815
Bankssts	24.4 (3.3)	25.9 (2.7)	26.1 (2.4)	0.085	0.072	0.681
Inferior temporal	19.7 (2.0)	22.9 (1.7)	24.2 (2.9)	**<0.001**	**<0.001**	**0.006**
Middle temporal	19.0 (1.9)	22.0 (1.8)	23.1 (3.1)	**<0.001**	**<0.001**	**0.011**
Superior temporal	20.3 (1.7)	22.9 (1.5)	23.7 (3.0)	**<0.001**	**<0.001**	**0.039**
Transverse temporal	32.5 (4.5)	34.8 (4.4)	35.0 (4.7)	**0.026**	**0.043**	0.815
Temporal pole	24.0 (2.5)	26.2 (2.4)	29.7 (4.5)	0.059	**<0.001**	**0.001**
Frontal Lobe						
Orbitofrontal	22.3 (2.7)	24.4 (1.9)	24.8 (2.8)	**<0.001**	**0.034**	0.946
Inferior frontal	24.4 (1.8)	25.6 (1.5)	26.1 (2.4)	**0.001**	**0.002**	0.211
Middle frontal	23.4 (2.0)	24.4 (2.0)	24.0 (2.7)	0.106	0.372	0.589
Superior frontal	20.7 (2.1)	21.8 (2.2)	21.8 (2.9)	0.057	0.171	0.982
Precentral	21.6 (1.6)	21.5 (2.4)	21.7 (2.1)	0.373	0.842	0.699
Paracentral	26.3 (2.7)	26.1 (3.0)	26.3 (4.6)	0.531	0.912	0.745
Frontal pole	28.1 (2.6)	29.2 (2.8)	31.6 (5.6)	0.078	**0.012**	**0.041**

Anterior cingulate	23.6 (2.0)	23.9 (1.6)	24.4 (2.6)	0.464	0.448	0.518
Parietal Lobe						
Inferior parietal	23.7 (2.3)	24.8 (2.5)	24.6 (2.2)	**0.048**	0.094	0.791
Superior parietal	25.4 (2.6)	26.0 (2.9)	26.3 (3.3)	0.596	0.282	0.555
Postcentral	25.6 (2.1)	25.1 (2.6)	25.5 (3.7)	0.148	0.965	0.392
Precuneus	23.9 (2.9)	23.8 (3.6)	22.5 (3.6)	0.319	0.060	0.144
Supra marginal	20.8 (1.7)	21.7 (2.0)	21.9 (2.2)	0.071	0.065	0.661
Isthmus cingulate	24.0 (1.9)	25.4 (2.4)	25.1 (2.8)	**0.007**	0.107	0.726
Posterior cingulate	24.6 (1.9)	26.2 (2.2)	26.1 (2.3)	**0.001**	**0.002**	0.980
Occipital Lobe						
Cuneus	36.0 (4.7)	34.4 (5.1)	33.4 (4.4)	0.055	0.063	0.589
Lingual	29.4 (3.5)	30.1 (3.2)	29.2 (4.2)	0.392	0.673	0.274
Lateral occipital	27.0 (3.3)	28.7 (2.3)	28.1 (3.0)	0.063	0.152	0.675
Pericalcarine	41.6 (6.6)	41.1 (5.4)	38.9 (6.0)	0.751	0.085	0.077
Subcortical Regions						
Accumbens area	27.4 (4.9)	26.2 (3.8)	25.8 (5.4)	0.377	0.274	0.749
Caudate	19.9 (1.8)	21.0 (2.2)	20.6 (3.8)	0.205	0.285	0.500
Putamen	22.5 (3.0)	23.8 (3.3)	23.4 (4.8)	0.133	0.122	0.842
Pallidum	25.4 (4.1)	26.6 (3.4)	26.1 (4.6)	0.158	0.588	0.676
Thalamus	14.9 (1.4)	15.3 (1.3)	14.8 (1.9)	0.339	0.871	0.413

Note. All values are presented as mean (standard deviation).

AD, Alzheimer's disease; SD, semantic dementia

*One-way analysis of covariance adjusting for corresponding regional volume with Bonferroni post hoc comparisons

Table 4. Logistic regression model parameters for differentiating patients with semantic dementia patients from normal controls

	Volume-based model*			Texture-based model*		
	B (SE)	p	95% CI	B (SE)	p	95% CI
Intercept	-4.708 (2.071)	-	-	-4.062 (0.915)	-	-
Amygdala						
Hippocampus						
Entorhinal	-2.029 (0.588)	0.001	0.042-0.417	1.773 (0.493)	<0.001	0.240-15.488
Para hippocampal						
Fusiform						
Bankssts						
Inferior temporal						
Middle temporal						
Superior temporal						
Transverse temporal						
Temporal pole	-1.105 (0.454)	0.015	0.136-0.806	1.309 (0.495)	0.008	1.405-9.762
Orbitofrontal						
Inferior frontal						
Middle frontal						
Superior frontal						
Precentral						
Paracentral						
Frontal pole	-0.853 (0.448)	0.057	0.177-1.026			
Anterior cingulate						

Inferior parietal
Superior parietal
Postcentral
Precuneus
Supra marginal
Isthmus cingulate
Posterior cingulate
Cuneus
Lingual
Lateral occipital
Pericalcarine
Accumbens area
Caudate
Putamen
Pallidum
Thalamus

B, regression coefficient; SE, standard error; CI, confidence interval

*Binary logistic regression analysis with forward selection

Table 5. Composite model parameters for differentiating normal controls from semantic dementia

		Composite model			
		B (SE)	p	OR	95% CI
	Intercept	-4.644 (1.175)	-	-	-
Volume	Entorhinal	-1.393 (0.745)	0.061	0.248	0.058-1.069
	Temporal pole	-0.590 (0.680)	0.386	0.554	0.146-2.102
	Frontal pole	-0.829 (0.666)	0.213	0.437	0.118-1.610
Texture	Entorhinal	1.018 (0.516)	0.048	2.766	1.007-7.600
	Temporal pole	1.119 (0.676)	0.098	3.063	0.815-11.515

B, regression coefficient; SE, standard error; OR, odds ratio; CI, confidence interval

Table 6. Performance metrics for volume, texture, and composite models in classifying normal controls from semantic dementia

	Sensitivity	Specificity	PPV	NPV	AUC
Volume-based model	0.800	0.950	0.889	0.905	0.963[a]
Texture-based model	0.867	1.000	1.000	0.938	0.966[b]
Composite model	0.867	0.983	0.963	0.937	0.983

PPV, positive predictive value; NPV, negative predictive value; AUC, area under curve

Pairwise AUC comparisons by Hanley & McNeil's method:

a) Volume-based model vs. Composite model, $p = 0.516$

b) Texture-based model vs. Composite model, $p = 0.557$

Table 7. Logistic regression model parameters for differentiating patients with semantic dementia patients from patients with Alzheimer's disease

	Volume-based model*			Texture-based model*		
	B (SE)	p	95% CI	B (SE)	p	95% CI
Intercept	-0.997(0.514)	-	-	-1.897 (0.465)	-	-
Amygdala						
Hippocampus	0.602 (0.223)	0.007	1.178-2.827	-0.618 (0.222)	0.005	0.349-0.833
Entorhinal						
Para hippocampal						
Fusiform						
Bankssts						
Inferior temporal						
Middle temporal						
Superior temporal						
Transverse temporal						
Temporal pole	-1.603 (2.256)	<0.001	0.209-0.570	0.982 (0.263)	<0.001	1.595-4.470
Orbitofrontal						
Inferior frontal						
Middle frontal						
Superior frontal						
Precentral						
Paracentral						
Frontal pole						
Anterior cingulate						

Inferior parietal
Superior parietal
Postcentral
Precuneus
Supra marginal
Isthmus cingulate
Posterior cingulate
Cuneus
Lingual
Lateral occipital
Pericalcarine
Accumbens area
Caudate
Putamen
Pallidum
Thalamus

B, regression coefficient; SE, standard error; CI, confidence interval

*Binary logistic regression analysis with forward selection

Table 8. Composite model parameters for differentiating Alzheimer's disease from semantic dementia

		Composite model			
		B (SE)	p	OR	95% CI
	Intercept	-1.743 (0.674)	-	-	-
Volume	Hippocampus	0.462 (0.251)	0.066	1.586	0.970-2.594
	Temporal pole	-0.834 (0.278)	0.003	0.434	0.252-0.749
Texture	Hippocampus	-0.529 (0.248)	0.033	0.589	0.362-0.959
	Temporal pole	0.718 (0.282)	0.011	2.050	1.180-3.561

B, regression coefficient; SE, standard error; OR, odds ratio; CI, confidence interval

Table 9. Performance metrics for volume, texture, and composite models in classifying Alzheimer's disease from semantic dementia

	Sensitivity	Specificity	PPV	NPV	AUC
Volume-based model	0.567	0.883	0.708	0.803	0.806 [a]
Texture-based model	0.533	0.917	0.762	0.797	0.816 [b]
Composite model	0.667	0.917	0.800	0.846	0.862

PPV, positive predictive value; NPV, negative predictive value; AUC, area under curve

Pairwise AUC comparisons by Hanley & McNeil's method:

a) Volume-based model vs. Composite model, $p = 0.418$

b) Texture-based model vs. Composite model, $p = 0.500$

Table 10. Demographic and clinical characteristics of the participants by diagnostic groups

	NC [a]	AD [b]	SNAP [c]	Statistics*	
	(n = 183)	(n = 164)	(n = 155)	*p*	Post-hoc
Age, years, mean (SD)	74.4 (4.5)	75.3 (4.4)	74.8 (4.4)	0.224	
Sex, female, %	63.4	51.4	61.9	0.102	
Education, years, mean (SD)	12.0 (4.8)	12.1 (5.0)	10.9 (5.2)	0.061	
Total brain volume†, cc, mean (SD)	985.5 (86.8)	980.7 (91.5)	962.7 (91.2)	0.055	
MMSE, points, mean (SD)	27.6 (2.1)	23.7 (4.1)	24.1 (3.5)	< 0.001	a > b, c

NC, normal cognition; AD, Alzheimer's disease; SNAP, Suspected Non-Alzheimer's Disease Pathophysiology; MMSE, Mini-Mental State Examination

†Sum of the volume of the structures identified in the Freesurfer aseg.mgz volume

*One-way analysis of variance for continuous variables and chi-square test for categorical variables with Bonferroni post hoc comparisons

Table 11. Comparison of regional volumes between diagnostic groups

	NC [a] (n = 183)	AD [b] (n = 164)	SNAP [c] (n = 155)	Statistics* NC-AD	NC-SNAP	AD-SNAP
Temporal Lobe						
Amygdala	2713.8 (364.8)	2396.4 (406.7)	2476.2 (512.8)	**<0.001**	**<0.001**	0.097
Hippocampus	7162.4 (680.0)	6278.9 (813.6)	6391.7 (893.0)	**<0.001**	**<0.001**	0.243
Entorhinal	3801.1 (600.2)	3228.6 (680.5)	3399.2 (834.9)	**<0.001**	**<0.001**	**0.044**
Para hippocampal	3311.4 (358.6)	3174.7 (519.3)	3211.3 (476.7)	0.061	0.140	0.585
Fusiform	16285.4 (1748.1)	15688.3 (2015.8)	15775.6 (1871.2)	0.159	0.196	0.843
Bankssts	3917.0 (502.3)	3729.9 (478.8)	3771.6 (555.6)	0.102	0.171	0.541
Inferior temporal	19237.2 (2607.8)	17977.5 (2559.3)	18068.7 (2742.8)	**0.001**	**0.001**	0.972
Middle temporal	19743.4 (2357.0)	18481.6 (2382.7)	18648.6 (2493.0)	**<0.001**	**0.001**	0.629
Superior temporal	20179.8 (2166.2)	19551.7 (2089.5)	19745.9 (2530.4)	0.263	0.902	0.503
Transverse temporal	1704.3 (270.0)	1636.3 (242.4)	1644.5 (262.6)	0.189	0.254	0.913
Temporal pole	4686.3 (513.1)	4550.5 (636.6)	4568.0 (688.7)	0.189	0.279	0.899
Frontal Lobe						
Orbitofrontal	21922.7 (2208.2)	21520.3 (2286.4)	21420.5 (2210.8)	0.315	0.758	0.233
Inferior frontal	17843.3 (2215.4)	17379.5 (2125.5)	17197.2 (1907.7)	0.995	0.099	0.151
Middle frontal	35335.3 (4079.9)	34246.6 (4165.5)	34892.9 (4396.5)	0.713	0.081	0.078
Superior frontal	36572.8 (3793.9)	35767.4 (3810.8)	36330.7 (3944.9)	0.718	0.057	0.124
Precentral	23811.7 (2408.7)	24221.9 (2798.5)	24364.6 (2663.4)	0.072	0.083	0.779
Paracentral	6798.7 (772.4)	6603.9 (828.3)	6713.3 (810.3)	0.436	0.668	0.224
Frontal pole	1868.6 (216.0)	1845.9 (228.2)	1837.0 (217.0)	0.970	0.501	0.623
Anterior cingulate	6946.1 (1060.4)	6714.9 (1110.5)	6689.6 (1123.5)	0.796	0.479	0.564

Parietal Lobe						
Inferior parietal	22894.6 (2911.9)	21976.3 (3069.7)	22322.1 (3021.4)	0.189	0.987	0.317
Superior parietal	22816.5 (2594.2)	22750.8 (3211.3)	23038.0 (2833.7)	0.230	0.067	0.451
Postcentral	16188.0 (1828.4)	15972.6 (1730.9)	16202.6 (1880.0)	0.292	0.073	0.235
Precuneus	16673.9 (1778.0)	15969.4 (1854.5)	16332.3 (1826.9)	**0.030**	0.995	**0.030**
Supra marginal	18239.7 (2108.0)	17473.6 (2302.7)	17895.7 (2166.3)	0.070	0.951	0.058
Isthmus cingulate	4400.2 (585.4)	4164.5 (600.0)	4287.1 (579.1)	0.103	0.625	0.055
Posterior cingulate	5503.6 (686.9)	5276.0 (842.6)	5300.9 (881.9)	0.180	0.219	0.961
Occipital Lobe						
Cuneus	5361.1 (752.4)	5275.5 (740.2)	5352.8 (757.4)	0.533	0.186	0.398
Lingual	11282.9 (1441.8)	10946.7 (1589.5)	10967.8 (1480.7)	0.680	0.406	0.909
Lateral occipital	19811.0 (2553.3)	19290.5 (2520.7)	19776.0 (2587.6)	0.792	0.069	0.073
Pericalcarine	3870.7 (715.8)	3852.5 (690.8)	3858.8 (690.5)	0.350	0.436	0.944
Subcortical Regions						
Accumbens area	836.3 (153.2)	795.8 (132.9)	786.0 (160.7)	0.075	0.077	0.405
Caudate	6462.1 (984.7)	6528.0 (1006.4)	6504.6 (1117.8)	0.063	0.149	0.726
Putamen	8404.7 (1090.0)	8304.6 (978.6)	8226.9 (1191.3)	0.416	0.883	0.324
Pallidum	3297.0 (411.5)	3309.5 (390.8)	3239.1 (447.6)	0.055	0.838	0.055
Thalamus	11740.5 (1119.0)	11482.4 (1112.4)	11470.2 (1118.8)	0.910	0.521	0.541

Note. All values are presented as mean (standard deviation) in mm^3.

NC, normal cognition; AD, Alzheimer's disease; SNAP, Suspected Non-Alzheimer's Disease Pathophysiology

*One-way analysis of covariance adjusting for total brain volume with Bonferroni post hoc comparisons

Table 12. Comparison of regional textures between diagnostic groups

	NC [a] (n = 183)	AD [b] (n = 164)	SNAP [c] (n = 155)	Statistics* NC-AD	NC-SNAP	AD-SNAP
Temporal Lobe						
Amygdala	24.2 (3.1)	24.7 (3.4)	24.8 (3.2)	**0.038**	**0.040**	0.549
Hippocampus	27.0 (2.0)	27.6 (2.9)	27.6 (2.2)	**0.027**	**0.035**	0.758
Entorhinal	25.8 (2.9)	29.5 (4.4)	29.0 (4.1)	**<0.001**	**<0.001**	0.938
Para hippocampal	26.9 (2.7)	29.6 (3.4)	28.9 (3.5)	**<0.001**	**<0.001**	0.077
Fusiform	23.3 (3.0)	24.1 (3.0)	24.1 (2.5)	0.060	**0.045**	0.920
Bankssts	24.5 (2.8)	26.7 (3.2)	25.6 (2.9)	**<0.001**	**0.001**	**0.004**
Inferior temporal	21.4 (2.2)	22.8 (2.3)	22.6 (2.2)	**<0.001**	**<0.001**	0.571
Middle temporal	20.3 (2.2)	21.8 (2.3)	21.5 (2.3)	**<0.001**	**<0.001**	0.196
Superior temporal	21.8 (2.0)	23.0 (1.8)	22.5 (1.7)	**<0.001**	**0.008**	**0.007**
Transverse temporal	34.3 (5.0)	35.7 (5.0)	35.7 (5.2)	0.058	0.061	0.990
Temporal pole	26.0 (2.0)	26.3 (3.1)	26.5 (2.8)	0.435	0.103	0.595
Frontal Lobe						
Orbitofrontal	23.2 (2.6)	23.9 (2.9)	23.3 (3.2)	0.069	0.716	0.108
Inferior frontal	24.7 (2.1)	25.8 (2.7)	25.8 (2.0)	**<0.001**	**<0.001**	0.832
Middle frontal	23.2 (2.0)	24.2 (2.2)	24.1 (2.0)	**<0.001**	**<0.001**	0.686
Superior frontal	20.6 (2.2)	21.6 (2.5)	22.3 (2.2)	**<0.001**	**<0.001**	**0.008**
Precentral	21.7 (2.0)	21.8 (2.4)	21.9 (2.3)	0.338	0.071	0.576
Paracentral	26.4 (3.4)	26.7 (3.5)	26.9 (3.7)	0.720	0.331	0.379
Frontal pole	28.5 (2.2)	29.1 (3.4)	29.0 (2.8)	0.073	0.076	0.706
Anterior cingulate	23.6 (2.1)	24.1 (1.9)	24.0 (1.7)	0.106	0.178	0.613

Parietal Lobe						
Inferior parietal	23.8 (2.2)	24.9 (2.5)	24.4 (2.2)	**<0.001**	0.105	0.116
Superior parietal	25.6 (2.5)	26.3 (3.1)	25.6 (2.6)	**0.043**	0.964	0.050
Postcentral	25.2 (2.7)	25.4 (2.9)	25.1 (2.6)	0.922	0.730	0.682
Precuneus	22.7 (3.0)	22.8 (3.5)	22.3 (3.1)	0.861	0.240	0.287
Supra marginal	21.2 (1.9)	22.0 (2.2)	21.6 (1.9)	**0.002**	0.062	0.178
Isthmus cingulate	24.1 (1.8)	24.9 (2.9)	24.3 (2.1)	**0.010**	0.445	**0.043**
Posterior cingulate	24.9 (1.8)	26.2 (2.5)	25.7 (1.9)	**<0.001**	**0.001**	**0.023**
Occipital Lobe						
Cuneus	34.0 (4.8)	33.1 (4.7)	33.0 (4.9)	0.107	0.116	0.808
Lingual	29.0 (3.2)	29.6 (3.1)	29.9 (3.4)	0.231	0.107	0.270
Lateral occipital	28.1 (2.7)	28.9 (2.8)	28.6 (2.5)	0.071	0.090	0.872
Pericalcarine	40.5 (6.0)	40.3 (4.9)	40.8 (5.4)	0.701	0.613	0.340
Subcortical Regions						
Accumbens area	27.7 (4.0)	26.9 (4.4)	26.5 (4.5)	0.059	**0.022**	0.486
Caudate	20.6 (2.1)	21.4 (2.5)	21.5 (2.0)	0.069	**0.031**	0.757
Putamen	23.4 (3.4)	25.0 (4.0)	25.4 (3.6)	0.081	**<0.001**	0.325
Pallidum	26.8 (3.8)	27.2 (4.2)	27.0 (3.9)	0.252	0.783	0.337
Thalamus	15.0 (1.4)	15.1 (2.0)	15.5 (1.5)	0.878	**0.002**	**0.020**

Note. All values are presented as mean (standard deviation).

NC, normal cognition; AD, Alzheimer's disease; SNAP, Suspected Non-Alzheimer's Disease Pathophysiology

*One-way analysis of covariance adjusting for corresponding regional volume with Bonferroni post hoc comparisons

Table 13. Logistic regression model parameters for classifying participants with Suspected Non-Alzheimer's Disease Pathophysiology from normal cognition

	Volume-based model*			Texture-based model*		
	B (SE)	p	95% CI	B (SE)	p	95% CI
Intercept	0.893 (0.155)	-	-	-1.138 (0.175)	-	-
Amygdala				0.818 (0.150)	<0.001	1.688-3.041
Hippocampus	-1.212 (0.149)	<0.001	0.222-0.399			
Entorhinal				0.797 (0.142)	<0.001	1.681-2.932
Para hippocampal						
Fusiform						
Bankssts						
Inferior temporal						
Middle temporal	-0.403 (0.165)	0.014	0.484-0.923			
Superior temporal						
Transverse temporal						
Temporal pole						
Orbitofrontal						
Inferior frontal						
Middle frontal						
Superior frontal				1.327 (0.231)	<0.001	2.396-5.929
Precentral						
Paracentral						
Frontal pole						
Anterior cingulate						

Inferior parietal			
Superior parietal			
Postcentral			
Precuneus			
Supra marginal			
Isthmus cingulate			
Posterior cingulate	0.345 (0.145)	0.017	1.063-1.875
Cuneus			
Lingual			
Lateral occipital			
Pericalcarine			
Accumbens area			
Caudate			
Putamen	0.564 (0.149)	<0.001	1.425-1.763
Pallidum			
Thalamus			

B, regression coefficient; SE, standard error; CI, confidence interval

*Binary logistic regression analysis with forward selection

Table 14. Composite model parameters for differentiating normal controls from Suspected Non-Alzheimer's Disease Pathophysiology

		Composite model*			
		B (SE)	p	OR	95% CI
	Intercept	-1.287 (0.185)	-	-	-
Volume	Hippocampus	-0.910 (0.168)	<0.001	0.402	0.289-0.560
	Middle frontal	-0.549 (0.183)	0.003	0.577	0.403-0.826
Texture	Amygdala	0.366 (0.175)	0.037	1.441	1.023-2.031
	Entorhinal	0.401 (0.163)	0.014	1.493	1.085-2.055
	Superior frontal	1.191 (0.242)	<0.001	3.291	2.047-5.291
	Posterior cingulate	0.133 (0.180)	0.458	1.143	0.803-1.625
	Putamen	0.257 (0.174)	0.140	1.293	0.919-1.820

B, regression coefficient; SE, standard error; OR, odds ratio; CI, confidence interval

Table 15. Performance metrics for volume, texture, and composite models in classifying normal controls from Suspected Non-Alzheimer's Disease Pathophysiology

	Sensitivity	Specificity	PPV	NPV	AUC
Volume-based model	0.645	0.787	0.719	0.724	0.778 [a*]
Texture-based model	0.690	0.814	0.759	0.756	0.838 [b]
Composite model	0.703	0.852	0.801	0.772	0.860

PPV, positive predictive value; NPV, negative predictive value; AUC, area under curve

Pairwise AUC comparisons by Hanley & McNeil's method:

a) Volume-based model vs. Composite model, $p = 0.014$

b) Texture-based model vs. Composite model, $p = 0.487$

*$p < 0.05$

Table 16. Logistic regression model parameters for classifying participants with Suspected Non-Alzheimer's Disease Pathophysiology from participants with Alzheimer's disease

	Volume-based model*			Texture-based model*		
	B (SE)	p	95% CI	B (SE)	p	95% CI
Intercept	0.088 (0.134)	-	-	-0.086 (0.155)	-	-
Amygdala						
Hippocampus						
Entorhinal	0.178 (0.090)	0.047	1.002-1.425			
Para hippocampal						
Fusiform						
Bankssts				-0.255 (0.148)	0.086	0.580-1.037
Inferior temporal						
Middle temporal						
Superior temporal				-0.454 (0.191)	0.018	0.437-0.924
Transverse temporal						
Temporal pole						
Orbitofrontal						
Inferior frontal						
Middle frontal						
Superior frontal				0.582 (0.154)	<0.001	1.323-2.421
Precentral						
Paracentral						
Frontal pole						
Anterior cingulate						

Inferior parietal			
Superior parietal	-0.406 (0.139)	0.004	0.507-0.876
Postcentral			
Precuneus			
Supra marginal			
Isthmus cingulate			
Posterior cingulate			
Cuneus			
Lingual			
Lateral occipital			
Pericalcarine			
Accumbens area			
Caudate			
Putamen			
Pallidum			
Thalamus	0.360 (0.115)	0.002	1.144-1.796

B, regression coefficient; SE, standard error; CI, confidence interval

*Binary logistic regression analysis with forward selection

Table 17. Composite model parameters for differentiating Alzheimer's disease from Suspected Non-Alzheimer's Disease Pathophysiology

		Composite model*			
		B (SE)	p	OR	95% CI
	Intercept	0.003 (0.170)	-	-	-
Volume	Entorhinal	0.130 (0.099)	0.189	1.139	0.938-1.383
Texture	Bankssts	-0.261 (0.149)	0.080	0.770	0.575-1.031
	Superior temporal	-0.391 (0.197)	0.047	0.676	0.460-0.998
	Superior frontal	0.568 (0.154)	<0.001	1.765	1.305-2.387
	Superior parietal	-0.428 (0.141)	0.002	0.652	0.494-0.859
	Thalamus	0.361 (0.115)	0.002	1.435	1.125-1.798

B, regression coefficient; SE, standard error; OR, odds ratio; CI, confidence interval

Table 18. Performance metrics for volume, texture, and composite models in classifying Alzheimer's disease from Suspected Non-Alzheimer's Disease Pathophysiology

	Sensitivity	Specificity	PPV	NPV	AUC
Volume-based model	0.458	0.671	0.568	0.567	0.567 [a**]
Texture-based model	0.632	0.659	0.636	0.655	0.693 [b]
Composite model	0.632	0.671	0.645	0.659	0.699

PPV, positive predictive value; NPV, negative predictive value; AUC, area under curve

Pairwise AUC comparisons by Hanley & McNeil's method:

a) Volume-based model vs. Composite model, $p = 0.002$

b) Texture-based model vs. Composite model, $p = 0.880$

**$p < 0.01$

A: Aggregated Aβ or associated pathologic state
CSF $A\beta_{42}$, or $A\beta_{42}/A\beta_{40}$ ratio
Amyloid PET
T: Aggregated tau (neurofibrillary tangles) or associated pathologic state
CSF phosphorylated tau
Tau PET
N: Neurodegeneration or neuronal injury
Anatomic MRI
FDG PET
CSF total tau

Figure 1. ATN biomarker grouping according to the NIA-AA framework

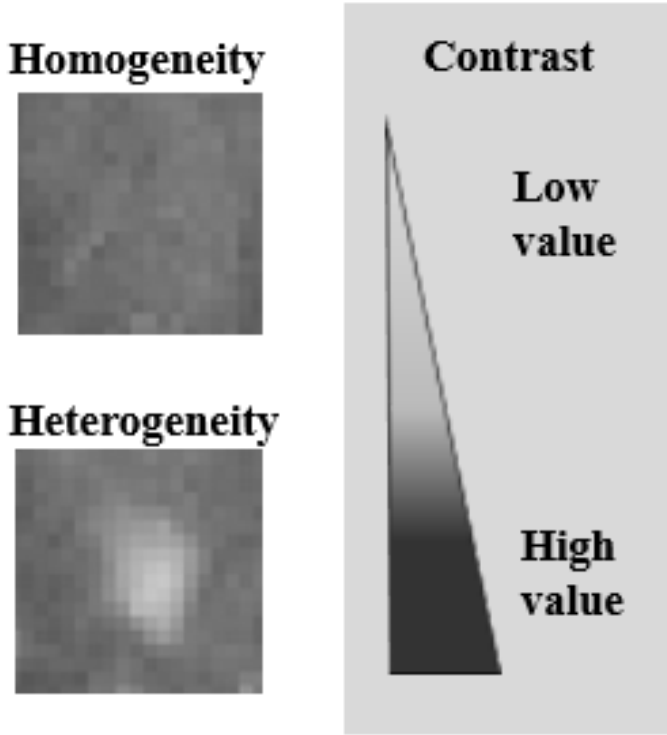

Figure 2. Illustration of homogeneity and heterogeneity in MRI scans with corresponding contrast scale

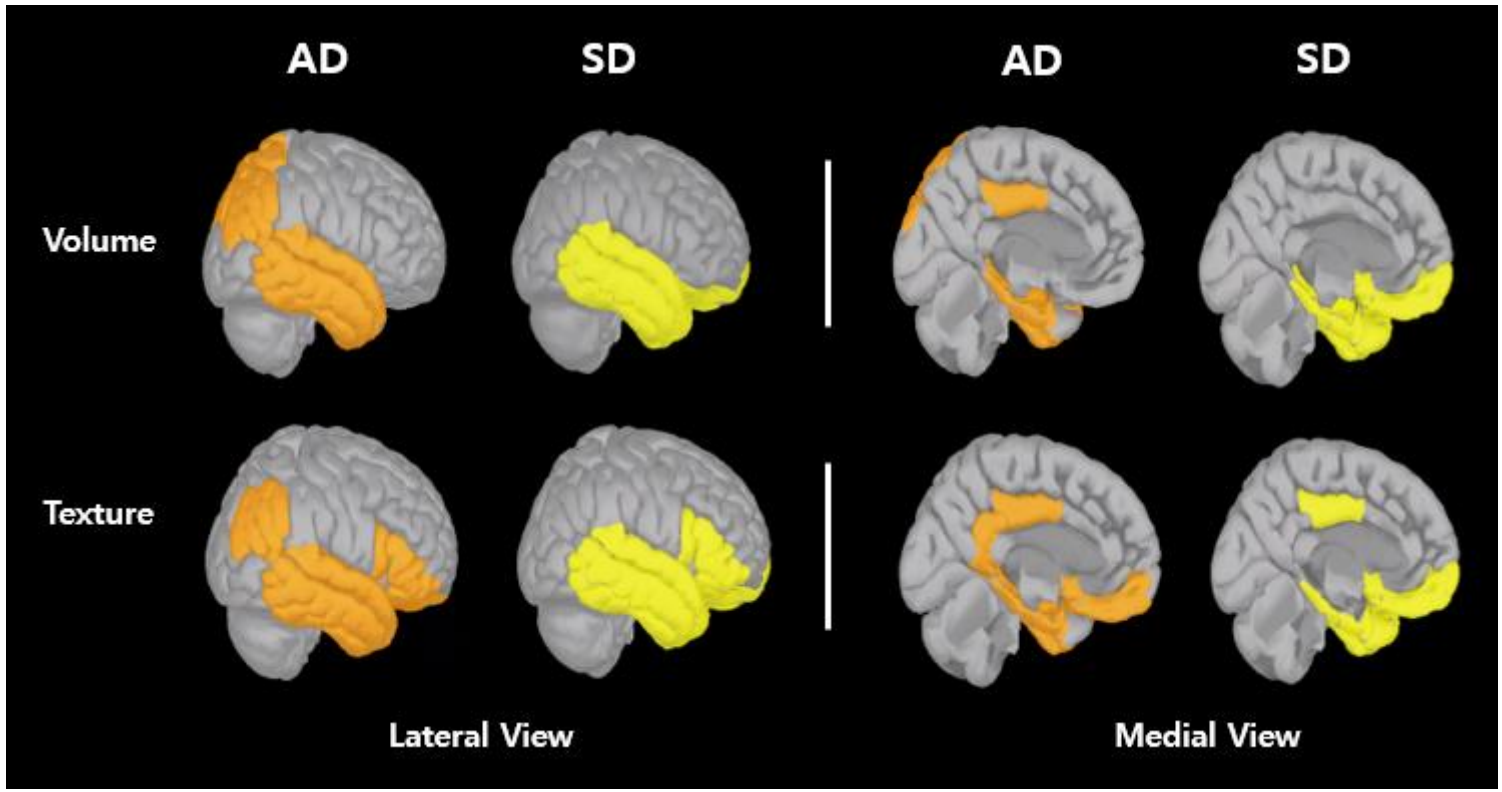

Figure 3. 3D brain visualization of regional volume and texture alterations in Alzheimer's disease and semantic dementia groups with lateral and medial views.

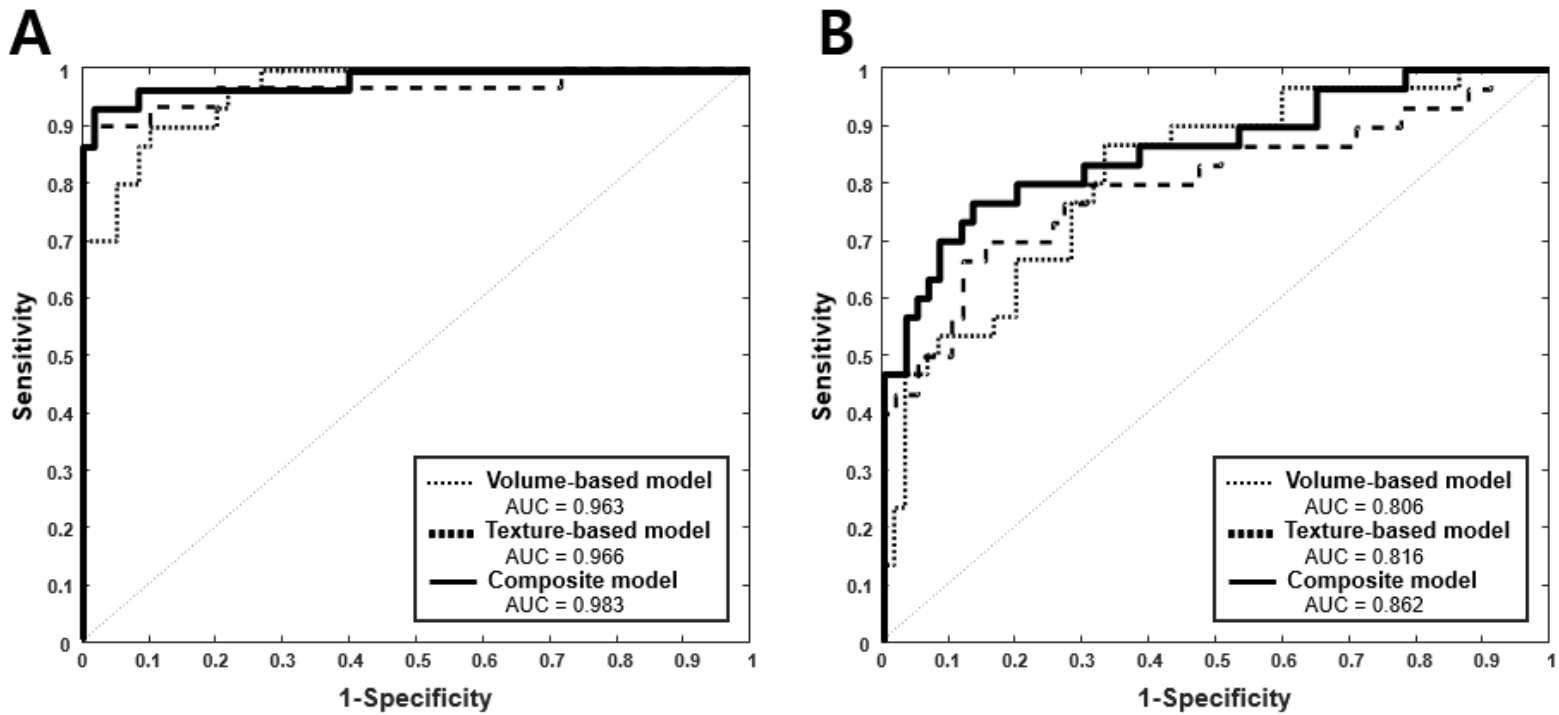

Figure 4. Comparison of the performance of the volume-based, texture-based and composite models for differentiating patients with semantic dementia from normal controls and patients with Alzheimer's disease

A. Models for differentiating patients semantic dementia from normal controls; B. Models for differentiating patients with semantic dementia from those with Alzheimer's disease

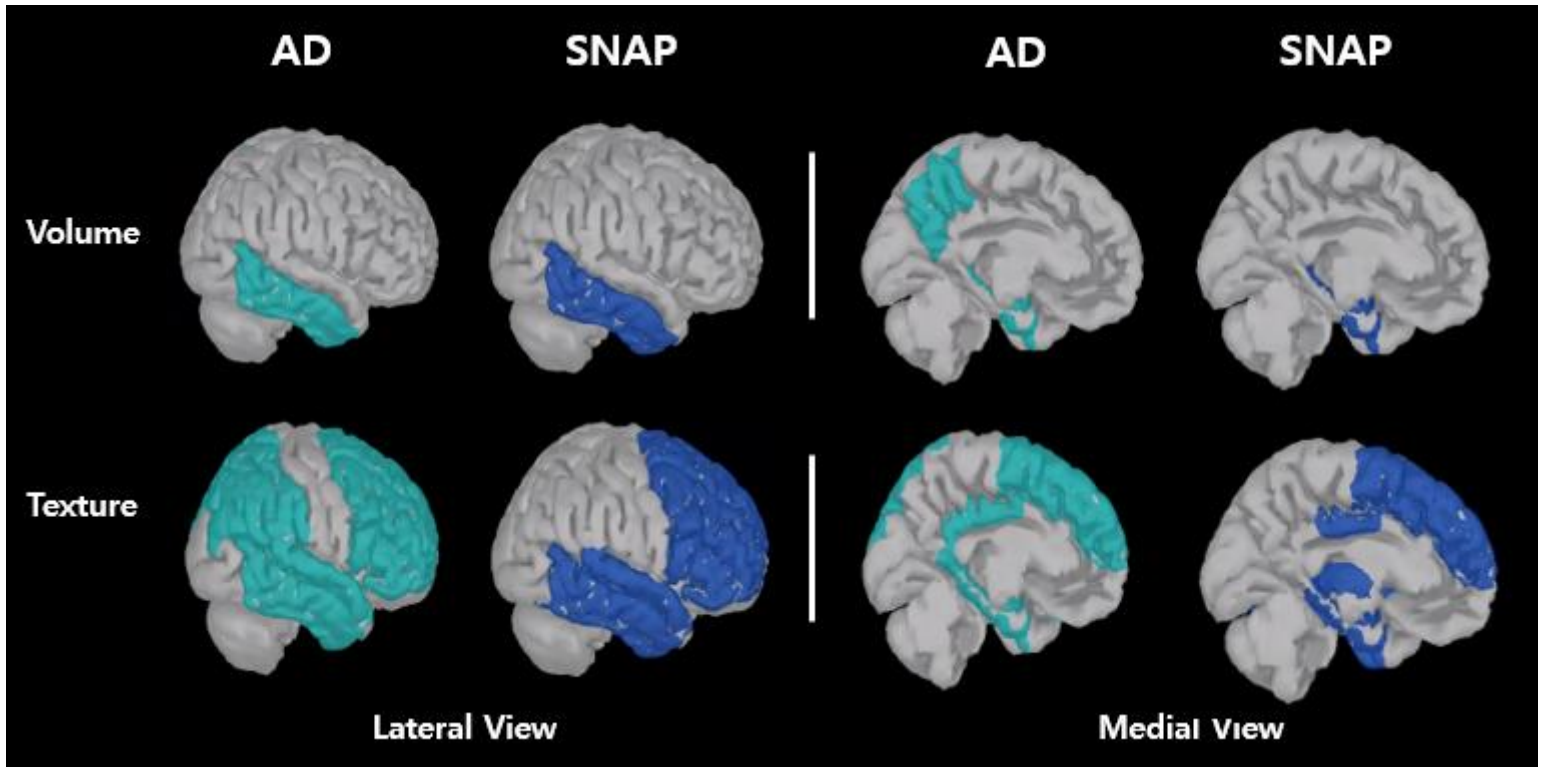

Figure 5. 3D brain visualization of regional volume and texture alterations in Alzheimer's Disease and Suspected Non-Alzheimer's Disease Pathophysiology groups with lateral and medial views.

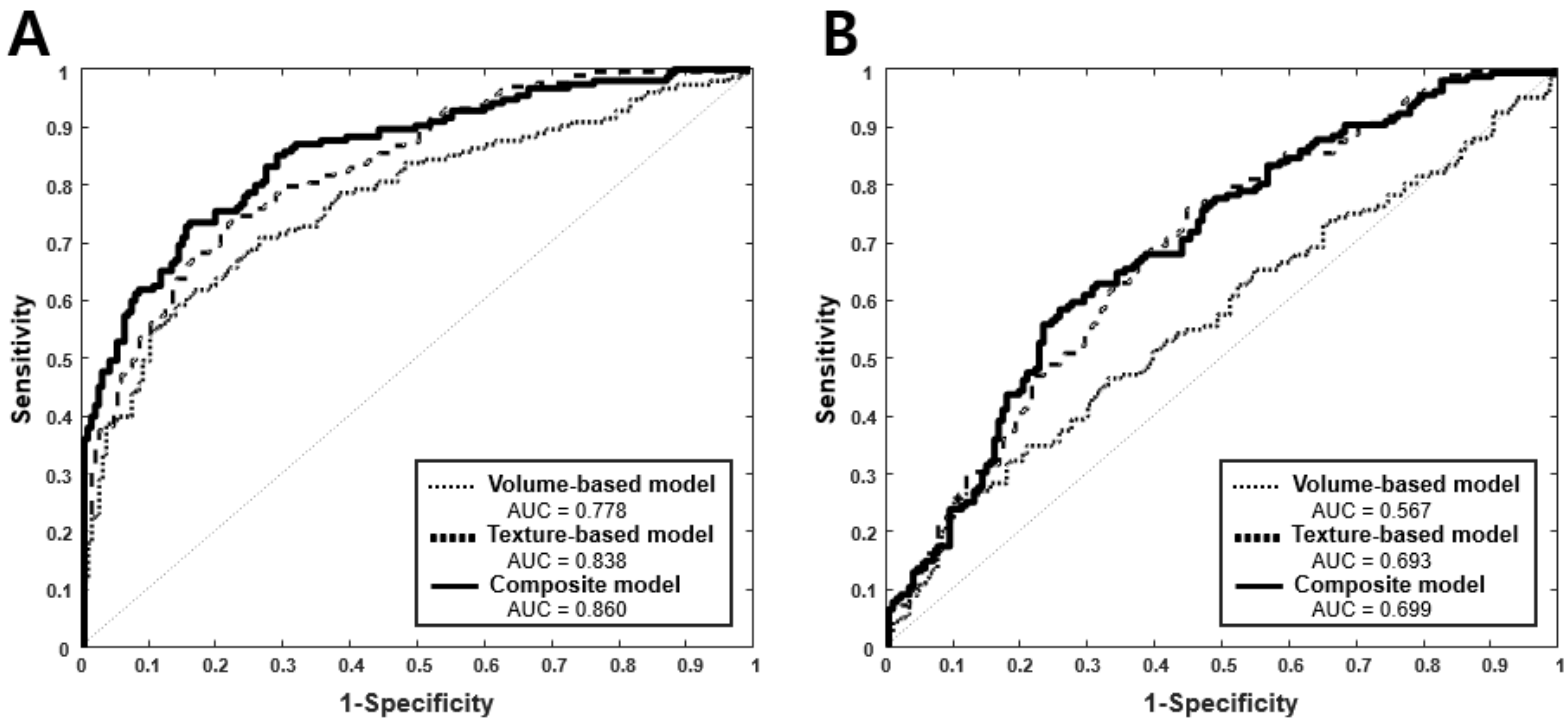

Figure 6. Comparison of the performance of the volume-based, texture-based and composite models for differentiating patients with Suspected Non-Alzheimer's Disease Pathophysiology from normal controls and Alzheimer's disease

A. Models for differentiating patients with Suspected Non-Alzheimer's Disease Pathophysiology from normal controls;

B. Models for differentiating patients with Suspected Non-Alzheimer's Disease Pathophysiology from those with Alzheimer's disease

Supplementary table 1. Cognitive performance scores for normal controls, Alzheimer's Disease and semantic dementia

	NC [a]	AD [b]	SD [c]	Statistics*	
	(n = 60)	(n = 60)	(n = 30)	*p*	Post-hoc
VFT, point	18.3 (4.3)	10.6 (4.3)	8.1 (3.8)	< 0.001	**a > b > c**
BNT, point	14.4 (0.8)	12.1 (2.8)	8.0 (4.0)	< 0.001	**a > b > c**
WLMT, point	19.8 (3.9)	11.1 (3.6)	11.1 (5.5)	< 0.001	a > b, c
WLRT, point	6.8 (2.1)	1.1 (1.4)	1.3 (2.0)	< 0.001	a > b, c
CPT, point	10.6 (0.7)	9.0 (1.8)	9.0 (2.0)	< 0.001	a > b, c
CRT, point	7.9 (2.6)	1.1 (1.6)	1.5 (1.7)	< 0.001	a > b, c
TMT-A, second	46.0 (21.7)	113.8 (99.6)	118.6 (84.9)	< 0.001	a > b, c
TMT-B, second	133.6 (75.9)	278.5 (98.0)	299.9 (103.8)	< 0.001	a > b, c
DST, point	13.7 (4.0)	9.8 (3.7)	9.5 (3.8)	< 0.001	a > b, c
FAB, point	16.6 (1.3)	11.7 (3.5)	10.7 (3.5)	< 0.001	a > b, c

Note. All values are presented as mean (standard deviation)

VFT, Verbal fluency test; BNT, Boston naming test; WLMT, Word list memory test; WLRT, Word list recall test; CPT, Constructional praxis test; CRT, Constructional recall test; TMT-A, Trail making test A; TMT-B, Trail making test B; DST, Digit span test; FAB, Frontal assessment battery

*One-way analysis of variance with Bonferroni post hoc comparisons

Supplementary table 2. Association of regional volume with cognitive performance in semantic dementia

	VFT	BNT	WLMT	WLRT	CPT	CRT	TMT-A	TMT-B	DST	FAB
Amygdala	-0.022	**.475***	0.223	0.225	0.230	-0.048	-0.358	-0.150	**.647****	0.236
Hippocampus	-0.234	0.187	0.237	0.140	0.093	0.014	-0.353	-0.028	**.530****	0.293
Entorhinal	0.244	**.488***	0.353	0.349	0.121	0.104	-0.323	-.470*	**.616****	0.265
Para hippocampal	-0.120	0.289	0.012	0.127	0.125	-0.040	-0.249	-0.281	**.445***	0.048
Fusiform	-0.144	0.058	0.063	0.196	0.196	0.005	-0.228	-0.386	0.176	-0.164
Bankssts	-0.176	0.084	-0.126	0.015	-0.105	-0.190	-0.105	-0.015	0.006	-0.382
Inferior temporal	0.051	0.305	0.142	0.342	0.161	0.211	-0.099	-0.363	0.009	-0.028
Middle temporal	0.090	0.225	0.175	0.327	0.128	0.267	-0.111	-0.288	-0.090	-0.114
Superior temporal	-0.095	0.227	0.033	0.131	0.083	0.074	-0.151	-0.070	0.237	-0.126
Transverse temporal	-0.119	-0.152	0.042	0.175	0.177	-0.120	0.009	0.224	0.324	-0.185
Temporal pole	0.070	0.346	0.228	0.251	0.214	0.388	-0.157	-0.355	0.263	0.171
Orbitofrontal	0.100	0.225	0.107	0.084	0.166	0.140	0.059	-0.130	0.155	-0.045
Inferior frontal	-0.295	-0.165	-0.311	-0.042	0.329	-0.256	-0.155	0.129	0.264	-0.136
Middle frontal	**-.411***	-0.097	-0.211	-0.106	0.381	-0.147	0.018	-0.021	0.300	-0.234
Superior frontal	-0.259	-0.044	-0.11	-0.120	0.382	-0.035	-0.056	0.072	0.291	-0.053
Precentral	-0.096	0.042	-0.261	-0.032	0.296	-0.180	-0.056	0.163	0.064	-0.132
Paracentral	-0.045	-0.123	-0.06	0.131	0.096	0.047	-0.063	-0.02	0.012	-0.321

Frontal pole	0.065	0.355	-0.004	-0.177	-0.036	0.237	0.251	-0.241	0.109	-0.061
Anterior cingulate	0.001	0.275	0.124	0.162	**.411***	0.198	-0.066	-0.302	0.374	0.035
Inferior parietal	-0.374	-0.096	-0.104	-0.033	0.066	-0.170	-0.084	0.045	0.061	-0.366
Superior parietal	-0.372	-0.030	-0.015	0.056	0.121	-0.178	-0.188	-0.093	0.091	-0.217
Postcentral	-.452*	0.055	-0.251	-0.308	0.121	-0.297	-0.111	0.242	0.393	-0.204
Precuneus	-0.238	-0.004	-0.083	0.125	0.277	-0.157	-0.248	-0.153	0.125	-0.191
Supra marginal	-0.369	-0.256	-0.248	-0.086	0.090	-0.188	0.243	0.240	-0.167	-.427*
Isthmus cingulate	-0.047	0.002	-0.157	0.034	0.358	-0.055	-0.174	-0.145	0.196	-0.186
Posterior cingulate	0.181	0.181	0.094	0.326	**.440***	0.186	-0.051	-0.28	0.261	-0.045
Cuneus	-0.377	0.158	-0.108	-0.180	**.413***	-0.106	-0.327	-0.136	**.520****	0.287
Lingual	-0.231	0.101	-0.052	-0.090	0.358	-0.070	**-.394***	-0.209	**.416***	0.114
Lateral occipital	**-.406***	-0.037	-0.197	-0.142	0.257	-0.251	-0.273	-0.105	0.305	-0.013
Pericalcarine	-0.188	0.228	-0.327	**-.394***	0.243	-0.124	-0.189	-0.120	**.602****	0.157
Accumbens area	0.357	0.301	0.325	0.274	-0.231	0.013	-0.288	**-.674****	0.170	0.130
Caudate	**-.394***	-0.021	-0.184	-0.208	0.164	-0.295	0.025	0.189	0.171	-0.193
Putamen	0.179	0.277	**.439***	0.177	0.032	0.196	-0.299	-0.137	0.206	0.203
Pallidum	**-.601****	-0.204	-0.073	-0.307	-0.069	-0.043	-0.133	**.407***	0.198	-0.062
Thalamus	**-.593****	-0.179	-0.171	-0.193	0.167	-0.195	0.000	0.322	0.335	0.069

***$p < 0.001$; **$p < 0.01$; *$p < 0.05$

Supplementary table 3. Association of regional texture with cognitive performance in semantic dementia

	VFT	BNT	WLMT	WLRT	CPT	CRT	TMT-A	TMT-B	DST	FAB
Amygdala	**.501****	-0.147	0.151	0.246	-0.253	0.213	0.265	-0.137	-0.401	-0.101
Hippocampus	0.188	0.206	-0.292	-0.316	-0.165	-0.089	0.087	0.033	-0.091	-0.171
Entorhinal	-0.064	-0.294	-0.146	-0.108	-0.324	-0.129	0.225	**.406***	-0.400	-0.261
Para hippocampal	0.190	-0.230	0.070	0.095	-0.133	0.030	0.375	0.119	**-.513***	-0.298
Fusiform	0.243	**-.449***	-0.093	0.012	-0.138	0.008	**.537****	0.120	-0.243	-0.254
Bankssts	-0.029	0.112	0.201	0.037	0.158	0.091	0.085	0.031	0.174	0.386
Inferior temporal	0.032	-0.110	-0.115	-0.174	-0.300	-0.249	0.330	0.215	-0.037	-0.131
Middle temporal	-0.087	-0.041	-0.172	-0.172	-0.249	-0.315	**.452***	0.100	-0.103	-0.095
Superior temporal	-0.092	-0.113	-0.229	-0.259	-0.285	-0.294	**.466***	0.047	-0.160	-0.153
Transverse temporal	-0.069	-0.015	-0.074	-0.287	-0.116	0.017	0.102	0.050	-0.145	0.043
Temporal pole	**-.395***	**-.409***	-0.314	-0.343	0.108	-0.349	-0.072	0.362	0.160	-0.188
Orbitofrontal	-0.297	-0.190	**-.425***	-0.354	-0.246	**-.463***	0.187	0.254	-0.207	-0.336
Inferior frontal	0.178	0.113	0.011	-0.086	-0.263	0.157	0.206	-0.003	-0.080	-0.153
Middle frontal	0.136	0.073	-0.071	-0.121	-0.285	-0.195	0.135	-0.159	-0.181	-0.111
Superior frontal	-0.126	-0.144	-0.231	-0.160	-0.357	-0.294	**.495***	-0.101	-0.336	-0.391
Precentral	-0.086	0.103	0.060	-0.064	-0.033	-0.176	-0.072	-0.140	-0.090	0.140
Paracentral	-0.120	-0.125	-0.209	-0.141	-0.042	0.022	**.599****	-0.176	-0.224	-0.184

Frontal pole	**-.514****	-0.359	-0.150	-0.299	0.159	-0.362	-0.118	0.395	0.339	0.003
Anterior cingulate	-0.247	-0.212	**-.397***	-0.308	-0.242	-0.343	0.379	0.137	**-.480***	-0.262
Inferior parietal	0.037	-0.008	-0.045	-0.159	-0.245	-0.210	0.304	0.041	0.185	-0.136
Superior parietal	0.084	0.089	-0.023	-0.098	0.030	-0.017	0.018	-0.248	0.089	0.040
Postcentral	0.144	0.033	0.042	-0.021	-0.053	-0.018	0.319	-0.175	-0.311	0.077
Precuneus	-0.064	-0.115	-0.178	-0.232	-0.108	-0.097	0.271	-0.047	-0.202	-0.214
Supra marginal	0.215	0.053	0.048	0.007	**-.419***	-0.124	0.152	-0.229	0.049	0.054
Isthmus cingulate	-0.071	-0.159	-0.069	-0.104	-0.263	-0.026	0.360	0.024	-0.253	-0.185
Posterior cingulate	-0.063	-0.093	-0.200	-0.312	**-.506****	-0.044	0.376	0.091	-0.186	-0.248
Cuneus	**.449***	0.136	0.319	**.397***	-0.120	0.289	0.105	0.003	-0.337	-0.003
Lingual	**.540****	0.156	0.228	0.262	-0.305	0.233	0.333	-0.137	-0.350	-0.069
Lateral occipital	0.386	-0.172	-0.039	0.117	-0.129	0.040	0.256	0.153	-0.359	-0.210
Pericalcarine	**.555****	0.041	0.101	0.241	-0.086	0.089	-0.042	0.040	-0.177	-0.030
Accumbens area	0.134	0.129	0.252	0.344	0.218	0.145	-0.022	0.102	-0.144	0.016
Caudate	0.375	-0.012	0.001	0.086	-0.289	0.151	**.456***	-0.175	**-.446***	-0.250
Putamen	0.299	0.143	-0.072	0.039	-0.161	-0.03	0.057	-0.165	-0.052	-0.229
Pallidum	0.311	-0.115	-0.092	0.046	-0.177	-0.115	-0.038	-0.180	-0.035	-0.251
Thalamus	0.216	0.135	0.038	-0.030	0.022	0.185	0.245	-0.161	-0.247	0.016

***$p < 0.001$; **$p < 0.01$; *$p < 0.05$

Supplementary table 4. Cognitive performance scores for normal controls, Alzheimer's Disease and Suspected Non-Alzheimer's Disease Pathophysiology

	NC [a]	AD [b]	SNAP [c]	Statistics*	
	(n = 183)	(n = 164)	(n = 155)	*p*	Post-hoc
VFT, point	17.7 (4.9)	11.9 (4.2)	12.1 (4.4)	< 0.001	a > b, c
BNT, point	12.7 (1.9)	12.1 (2.4)	11.7 (2.1)	< 0.001	a > b, c
WLMT, point	19.1 (3.9)	12.6 (3.6)	13.6 (3.7)	< 0.001	a > b, c
WLRT, point	6.2 (2.0)	1.7 (1.8)	2.7 (1.9)	< 0.001	**a > c > b**
CPT, point	10.2 (1.1)	9.5 (1.6)	9.6 (1.3)	< 0.001	a > b, c
CRT, point	7.2 (2.7)	2.8 (2.7)	3.5 (3.0)	< 0.001	a > b, c
TMT-A, second	50.1 (23.6)	81.2 (66.6)	72.6 (51.7)	< 0.001	a > b, c
TMT-B, second	156.4 (83.6)	248.1 (104.5)	243.6 (99.6)	< 0.001	a > b, c
DST, point	10.3 (2.4)	9.9 (3.4)	9.3 (2.4)	0.004	a > c
FAB, point	15.8 (1.8)	13.6 (3.0)	13.4 (2.6)	< 0.001	a > b, c

Note. All values are presented as mean (standard deviation)

VFT, Verbal fluency test; BNT, Boston naming test; WLMT, Word list memory test; WLRT, Word list recall test; CPT, Constructional praxis test; CRT, Constructional recall test; TMT-A, Trail making test A; TMT-B, Trail making test B; DST, Digit span test; FAB, Frontal assessment battery

*One-way analysis of variance with Bonferroni post hoc comparisons

Supplementary table 5. Association of regional volume with cognitive performance in Suspected Non-Alzheimer's Disease Pathophysiology

	VFT	BNT	WLMT	WLRT	CPT	CRT	TMT-A	TMT-B	DST	FAB
Amygdala	**.189***	0.029	0.080	**.170***	**.215****	**.269****	-0.119	-0.132	-0.036	0.056
Hippocampus	**.191***	0.006	**.175***	**.316****	**.229****	**.393****	-0.148	-0.112	0.048	0.102
Entorhinal	**.236****	0.056	0.115	**.199***	**.226****	**.333****	-0.117	-0.114	0.001	0.100
Para hippocampal	**.332****	0.084	0.112	**.267****	**.177***	**.228****	**-.207****	-0.153	-0.018	0.138
Fusiform	**.221****	-0.015	**.279****	**.314****	**.200***	**.292****	**-.201***	**-.174***	0.073	**.228****
Bankssts	**.272****	0.052	**.158***	**.285****	**.242****	**.278****	**-.242****	**-.231****	0.036	**.217****
Inferior temporal	**.174***	0.042	0.123	**.198***	**.168***	**.191***	**-.187***	**-.229****	-0.021	0.145
Middle temporal	0.153	0.032	0.098	0.136	**.173***	**.172***	**-.209****	-0.155	-0.044	**.164***
Superior temporal	**.231****	0.046	0.086	0.143	**.256****	**.191***	**-.201***	**-.188***	-0.020	0.119
Transverse temporal	0.106	0.099	0.027	0.042	0.096	0.049	-0.079	-0.082	-0.086	0.009
Temporal pole	-0.017	0.082	0.062	0.045	0.093	0.031	-0.046	0.112	-0.075	0.047
Orbitofrontal	**.204***	0.152	0.083	0.140	**.265****	0.150	**-.210****	**-.229****	0.063	0.111
Inferior frontal	0.081	0.095	0.031	0.074	**.194***	0.112	-0.072	-0.126	-0.015	0.041
Middle frontal	0.111	0.128	0.009	0.057	**.178***	0.142	-0.076	-0.159	0.013	0.051
Superior frontal	0.019	0.124	0.04	0.005	**.177***	0.069	-0.061	-0.034	0.013	0.004
Precentral	**.166***	0.046	0.077	0.156	0.136	0.107	-0.125	-0.111	0.061	0.083
Paracentral	0.121	0.157	0.093	0.157	**.170***	0.139	-0.044	-0.047	0.039	0.008

Frontal pole	-0.066	**.173***	0.016	-0.024	0.037	-0.003	0.023	-0.010	-0.064	-0.103
Anterior cingulate	0.146	0.084	0.085	0.139	**.303****	**.193***	**-.197***	**-.198***	0.066	0.093
Inferior parietal	0.149	0.102	**.161***	**.172***	**.173***	**.188***	-0.081	**-.211****	0.145	**.159***
Superior parietal	**.158***	0.128	0.055	0.065	**.181***	0.139	-0.076	-0.114	0.145	0.026
Postcentral	0.023	0.009	-0.023	0.009	0.096	0.053	0.036	-0.036	-0.053	-0.038
Precuneus	**.184***	0.145	0.107	**.159***	**.193***	**.208****	-0.108	**-.195***	0.059	0.064
Supra marginal	**.219****	**.158***	0.133	0.123	**.171***	0.121	**-.236****	**-.241****	0.012	**.187***
Isthmus cingulate	**.184***	0.021	0.025	**.161***	**.181***	**.237****	-0.127	-0.144	-0.070	0.140
Posterior cingulate	**.169***	-0.008	0.110	0.085	**.229****	0.123	**-.207***	-0.144	0.056	**.192***
Cuneus	0.030	0.124	0.045	0.091	**.215****	**.170***	-0.137	**-.240****	0.094	0.120
Lingual	0.077	0.147	-0.069	0.068	**.158***	0.137	-0.024	-0.148	0.108	0.012
Lateral occipital	0.051	0.079	0.142	0.099	**.223****	0.151	**-.170***	**-.218****	0.103	**.205***
Pericalcarine	0.024	0.072	-0.048	0.010	0.151	0.113	-0.031	-0.102	0.061	-0.022
Accumbens area	**.161***	0.139	0.033	**.189***	0.092	**.238****	0.005	-0.117	-0.005	-0.001
Caudate	-0.070	0.080	-0.097	-0.059	0.029	0.042	**.297****	-0.045	-0.011	0.010
Putamen	0.046	0.028	-0.010	0.054	0.052	0.078	**.199***	-0.050	-0.071	-0.027
Pallidum	0.156	0.055	0.031	0.115	**.214****	0.154	0.019	**-.182***	0.068	0.047
Thalamus	0.122	0.085	0.124	**.165***	**.232****	**.274****	-0.136	**-.235****	**.174***	0.142

***$p < 0.001$; **$p < 0.01$; *$p < 0.05$

Supplementary table 6. Association of regional texture with cognitive performance Suspected Non-Alzheimer's Disease Pathophysiology

	VFT	BNT	WLMT	WLRT	CPT	CRT	TMT-A	TMT-B	DST	FAB
Amygdala	-0.059	-0.155	-0.148	**-.171***	0.045	-0.072	0.005	-0.003	-0.132	0.062
Hippocampus	-0.034	-0.028	-0.057	-0.049	0.010	-0.043	0.047	0.088	-0.068	-0.004
Entorhinal	-0.134	-0.146	**-.221****	**-.291****	-0.112	**-.282****	0.081	0.035	0.022	-0.003
Para hippocampal	-0.090	-0.132	-0.028	**-.228****	-0.032	-0.123	-0.006	-0.047	0.074	0.051
Fusiform	0.000	-0.054	-0.062	-0.094	-0.033	-0.060	0.054	-0.016	-0.111	0.065
Bankssts	0.006	-0.040	-0.006	-0.074	-0.028	-0.072	0.009	-0.026	0.074	0.038
Inferior temporal	-0.068	-0.043	-0.124	-0.156	**-.176***	-0.127	**.199***	0.100	-0.035	-0.074
Middle temporal	-0.085	-0.114	-0.157	**-.197***	**-.208****	**-.189***	**.174***	0.132	-0.074	-0.122
Superior temporal	-0.087	-0.131	-0.155	**-.174***	-0.128	**-.172***	**.201***	0.148	-0.118	-0.078
Transverse temporal	-0.129	**-.242****	-0.043	-0.098	-0.089	-0.056	-0.024	0.117	-0.126	-0.085
Temporal pole	-0.019	0.017	-0.094	-0.063	-0.017	-0.032	-0.011	-0.034	0.073	0.008
Orbitofrontal	-0.023	-0.007	-0.043	-0.036	0.023	-0.054	0.121	0.125	-0.020	-0.107
Inferior frontal	-0.017	-0.028	-0.069	-0.097	-0.048	-0.034	0.028	0.114	-0.064	-0.062
Middle frontal	0.021	-0.073	0.035	0.001	0.054	0.014	-0.003	-0.029	-0.029	0.090
Superior frontal	0.033	-0.059	0.061	-0.051	0.036	-0.019	-0.028	-0.13	-0.082	0.055
Precentral	-0.022	-0.103	0.015	-0.012	-0.006	-0.013	-0.016	0.026	-0.117	0.099
Paracentral	-0.043	-0.132	-0.067	-0.067	0.110	-0.004	0.034	-0.003	-0.057	0.056

Frontal pole	0.059	-0.105	0.086	0.100	0.103	0.064	-0.018	-0.038	-0.027	0.065
Anterior cingulate	-0.053	-0.112	0.000	0.004	0.024	0.036	0.083	-0.007	0.036	0.004
Inferior parietal	-0.025	-0.101	-0.007	-0.058	0.097	-0.045	-0.049	-0.006	0.034	-0.001
Superior parietal	0.116	-0.096	0.073	0.055	**.174***	0.039	-0.139	-0.088	0.035	**.160***
Postcentral	0.077	-0.078	0.099	0.093	0.070	0.008	-0.126	-0.060	-0.059	**.213****
Precuneus	0.051	-0.082	0.097	0.052	0.157	0.042	-0.036	-0.016	0.059	0.082
Supra marginal	-0.061	**-.251****	-0.072	-0.081	-0.085	-0.015	0.088	**.171***	-0.065	-0.032
Isthmus cingulate	-0.001	**-.203***	0.056	-0.058	0.015	-0.050	-0.020	0.042	0.009	0.049
Posterior cingulate	-0.079	-0.039	-0.12	**-.181***	-0.017	-0.043	0.141	0.034	-0.047	-0.122
Cuneus	0.109	-0.078	**.176***	0.099	0.034	0.074	-0.062	-0.011	0.002	0.130
Lingual	-0.085	**-.176***	0.051	-0.019	-0.010	-0.058	0.006	0.077	-0.133	0.026
Lateral occipital	0.031	-0.147	-0.103	-0.050	0.050	0.011	0.020	0.072	-0.095	-0.063
Pericalcarine	0.054	-0.133	0.088	0.037	0.045	-0.050	-0.053	-0.019	0.048	0.077
Accumbens area	0.135	0.118	**.207****	0.135	0.066	0.073	-0.158	**-.234****	0.087	**.164***
Caudate	-0.043	-0.094	**-.166***	-0.099	-0.123	-0.140	-0.048	-0.027	-0.013	**-.183***
Putamen	0.047	-0.125	-0.06	-0.116	-0.034	-0.021	-0.049	-0.030	0.067	0.062
Pallidum	0.046	-0.102	0.035	-0.008	-0.069	-0.015	-0.100	0.088	0.056	0.102
Thalamus	-0.123	-0.076	-0.031	-0.129	-0.073	-0.089	0.140	0.065	-0.010	-0.017

***$p < 0.001$; **$p < 0.01$; *$p < 0.05$

Bibliography

Barthel, H., Gertz, H. J., Dresel, S., Peters, O., Bartenstein, P., Buerger, K., Hiemeyer, F., Wittemer-Rump, S. M., Seibyl, J., Reininger, C., Sabri, O., & Florbetaben Study, G. (2011). Cerebral amyloid-beta PET with florbetaben (18F) in patients with Alzheimer's disease and healthy controls: a multicentre phase 2 diagnostic study. *Lancet Neurol*, *10*(5), 424-435. https://doi.org/10.1016/S1474-4422(11)70077-1

Basso, M., Yang, J., Warren, L., MacAvoy, M. G., Varma, P., Bronen, R. A., & van Dyck, C. H. (2006). Volumetry of amygdala and hippocampus and memory performance in Alzheimer's disease. *Psychiatry Research: Neuroimaging*, *146*(3), 251-261.

Bell, C. C. (1994). DSM-IV: diagnostic and statistical manual of mental disorders. *Jama*, *272*(10), 828-829.

Borghammer, P., Østergaard, K., Cumming, P., Gjedde, A., Rodell, A., Hall, N., & Chakravarty, M. (2010). A deformation-based morphometry study of patients with early-stage Parkinson's disease. *European journal of neurology*, *17*(2), 314-320.

Burnham, S. C., Bourgeat, P., Doré, V., Savage, G., Brown, B., Laws, S., Maruff, P., Salvado, O., Ames, D., & Martins, R. N. (2016). Clinical and cognitive trajectories in cognitively healthy elderly individuals with suspected non-Alzheimer's disease pathophysiology (SNAP) or Alzheimer's disease pathology: a longitudinal study. *The Lancet Neurology*, *15*(10), 1044-1053.

Burton, E. J., Karas, G., Paling, S., Barber, R., Williams, E. D., Ballard, C., McKeith, I. G., Scheltens, P., Barkhof, F., & O'Brien, J. T. (2002). Patterns of cerebral atrophy in dementia with Lewy bodies using voxel-based morphometry. *Neuroimage*, *17*(2), 618-630.

Cairns, N. J., Neumann, M., Bigio, E. H., Holm, I. E., Troost, D., Hatanpaa, K. J., Foong, C., White III, C. L., Schneider, J. A., & Kretzschmar, H. A. (2007). TDP-43 in familial and sporadic frontotemporal lobar degeneration with ubiquitin inclusions. *The American journal of pathology*, *171*(1), 227-240.

Camicioli, R., Gee, M., Bouchard, T. P., Fisher, N. J., Hanstock, C. C., Emery, D. J., & Martin,

W. W. (2009). Voxel-based morphometry reveals extra-nigral atrophy patterns associated with dopamine refractory cognitive and motor impairment in parkinsonism. *Parkinsonism & related disorders*, *15*(3), 187-195.

Chung, J. K., Plitman, E., Nakajima, S., Caravaggio, F., Iwata, Y., Gerretsen, P., Kim, J., Takeuchi, H., Shinagawa, S., & Patel, R. (2017). Hippocampal and clinical trajectories of mild cognitive impairment with suspected non-Alzheimer's disease pathology. *Journal of Alzheimer's Disease*, *58*(3), 747-762.

Collewet, G., Strzelecki, M., & Mariette, F. (2004). Influence of MRI acquisition protocols and image intensity normalization methods on texture classification. *Magnetic resonance imaging*, *22*(1), 81-91.

Collins, J. A., Montal, V., Hochberg, D., Quimby, M., Mandelli, M. L., Makris, N., Seeley, W. W., Gorno-Tempini, M. L., & Dickerson, B. C. (2017). Focal temporal pole atrophy and network degeneration in semantic variant primary progressive aphasia. *Brain*, *140*(2), 457-471. https://www.ncbi.nlm.nih.gov/pmc/articles/PMC5278308/pdf/aww313.pdf

Cousins, D., Burton, E., Burn, D., Gholkar, A., McKeith, I., & O'Brien, J. (2003). Atrophy of the putamen in dementia with Lewy bodies but not Alzheimer's disease: an MRI study. *Neurology*, *61*(9), 1191-1195.

Coyle-Gilchrist, I. T., Dick, K. M., Patterson, K., Vázquez Rodríquez, P., Wehmann, E., Wilcox, A., Lansdall, C. J., Dawson, K. E., Wiggins, J., & Mead, S. (2016). Prevalence, characteristics, and survival of frontotemporal lobar degeneration syndromes. *Neurology*, *86*(18), 1736-1743.

Dani, M., Brooks, D. J., & Edison, P. (2017). Suspected non-Alzheimer's pathology–Is it non-Alzheimer's or non-amyloid? *Ageing Research Reviews*, *36*, 20-31.

Davidson, Y., Kelley, T., Mackenzie, I. R., Pickering-Brown, S., Du Plessis, D., Neary, D., Snowden, J. S., & Mann, D. M. (2007). Ubiquitinated pathological lesions in frontotemporal lobar degeneration contain the TAR DNA-binding protein, TDP-43. *Acta neuropathologica*, *113*, 521-533.

Does, M. D. (2018). Inferring brain tissue composition and microstructure via MR relaxometry. *Neuroimage*, *182*, 136-148.

Douglas, W., & Scharre, M. (2019). Preclinical, prodromal, and dementia stages of Alzheimer's disease. *Pract. Neurol*, *2019*, 36-42.

Eickhoff, S., Walters, N. B., Schleicher, A., Kril, J., Egan, G. F., Zilles, K., Watson, J. D., & Amunts, K. (2005). High-resolution MRI reflects myeloarchitecture and

cytoarchitecture of human cerebral cortex. *Human brain mapping*, *24*(3), 206-215.

Fazekas, F., Chawluk, J. B., Alavi, A., Hurtig, H. I., & Zimmerman, R. A. (1987). MR signal abnormalities at 1.5 T in Alzheimer's dementia and normal aging. *American Journal of Neuroradiology*, *8*(3), 421-426.

Fischl, B., Salat, D. H., Busa, E., Albert, M., Dieterich, M., Haselgrove, C., Van Der Kouwe, A., Killiany, R., Kennedy, D., & Klaveness, S. (2002). Whole brain segmentation: automated labeling of neuroanatomical structures in the human brain. *Neuron*, *33*(3), 341-355. https://www.cell.com/neuron/pdf/S0896-6273(02)00569-X.pdf

Geser, F., Martinez-Lage, M., Robinson, J., Uryu, K., Neumann, M., Brandmeir, N. J., Xie, S. X., Kwong, L. K., Elman, L., & McCluskey, L. (2009). Clinical and pathological continuum of multisystem TDP-43 proteinopathies. *Archives of neurology*, *66*(2), 180-189.

Gordon, B. A., Blazey, T., Su, Y., Fagan, A. M., Holtzman, D. M., Morris, J. C., & Benzinger, T. L. (2016). Longitudinal β-amyloid deposition and hippocampal volume in preclinical Alzheimer disease and suspected non–Alzheimer disease pathophysiology. *JAMA neurology*, *73*(10), 1192-1200.

Guo, X., Wang, Z., Li, K., Li, Z., Qi, Z., Jin, Z., Yao, L., & Chen, K. (2010). Voxel-based assessment of gray and white matter volumes in Alzheimer's disease. *Neuroscience letters*, *468*(2), 146-150.

Han, J. W., Kim, T. H., Kwak, K. P., Kim, K., Kim, B. J., Kim, S. G., Kim, J. L., Kim, T. H., Moon, S. W., Park, J. Y., Park, J. H., Byun, S., Suh, S. W., Seo, J. Y., So, Y., Ryu, S. H., Youn, J. C., Lee, K. H., Lee, D. Y., . . . Kim, K. W. (2018). Overview of the Korean Longitudinal Study on Cognitive Aging and Dementia. *Psychiatry Investig*, *15*(8), 767-774. https://doi.org/10.30773/pi.2018.06.02

Hanley, J. A., & McNeil, B. J. (1983). A method of comparing the areas under receiver operating characteristic curves derived from the same cases. *Radiology*, *148*(3), 839-843.

Haralick, R. M., Shanmugam, K., & Dinstein, I. H. (1973). Textural features for image classification. *IEEE Transactions on systems, man, and cybernetics*(6), 610-621.

Hodges, J. R., Mitchell, J., Dawson, K., Spillantini, M. G., Xuereb, J. H., McMonagle, P., Nestor, P. J., & Patterson, K. (2010). Semantic dementia: demography, familial factors and survival in a consecutive series of 100 cases. *Brain*, *133*(1), 300-306.

Jack Jr, C. R., Bennett, D. A., Blennow, K., Carrillo, M. C., Dunn, B., Haeberlein, S. B.,

Holtzman, D. M., Jagust, W., Jessen, F., & Karlawish, J. (2018a). NIA-AA research framework: toward a biological definition of Alzheimer's disease. *Alzheimer's & Dementia*, *14*(4), 535-562.

Jack Jr, C. R., Bennett, D. A., Blennow, K., Carrillo, M. C., Dunn, B., Haeberlein, S. B., Holtzman, D. M., Jagust, W., Jessen, F., & Karlawish, J. (2018b). NIA-AA research framework: toward a biological definition of Alzheimer's disease. *Alzheimer's & Dementia*, *14*(4), 535-562.

Jack Jr, C. R., Knopman, D. S., Chételat, G., Dickson, D., Fagan, A. M., Frisoni, G. B., Jagust, W., Mormino, E. C., Petersen, R. C., & Sperling, R. A. (2016). Suspected non-Alzheimer disease pathophysiology—concept and controversy. *Nature Reviews Neurology*, *12*(2), 117-124.

Jack Jr, C. R., Knopman, D. S., Weigand, S. D., Wiste, H. J., Vemuri, P., Lowe, V., Kantarci, K., Gunter, J. L., Senjem, M. L., & Ivnik, R. J. (2012). An operational approach to National Institute on Aging–Alzheimer's Association criteria for preclinical Alzheimer disease. *Annals of neurology*, *71*(6), 765-775.

Janelidze, S., Zetterberg, H., Mattsson, N., Palmqvist, S., Vanderstichele, H., Lindberg, O., van Westen, D., Stomrud, E., Minthon, L., & Blennow, K. (2016). CSF Aβ42/Aβ40 and Aβ42/Aβ38 ratios: better diagnostic markers of Alzheimer disease. *Annals of clinical and translational neurology*, *3*(3), 154-165.

Josephs, K. A., Hodges, J. R., Snowden, J. S., Mackenzie, I. R., Neumann, M., Mann, D. M., & Dickson, D. W. (2011). Neuropathological background of phenotypical variability in frontotemporal dementia. *Acta neuropathologica*, *122*(2), 137-153. https://www.ncbi.nlm.nih.gov/pmc/articles/PMC3232515/pdf/401_2011_Article_839.pdf

Klein, A., & Tourville, J. (2012). 101 labeled brain images and a consistent human cortical labeling protocol. *Frontiers in neuroscience*, *6*, 171.

Klunk, W. E., Engler, H., Nordberg, A., Wang, Y., Blomqvist, G., Holt, D. P., Bergström, M., Savitcheva, I., Huang, G. F., & Estrada, S. (2004). Imaging brain amyloid in Alzheimer's disease with Pittsburgh Compound-B. *Annals of Neurology: Official Journal of the American Neurological Association and the Child Neurology Society*, *55*(3), 306-319.

Kwon, M. J., Lee, S., Park, J., Jo, S., Han, J. W., Oh, D. J., Lee, J.-Y., Park, J. H., Kim, J. H., & Kim, K. W. (2023). Textural and Volumetric Changes of the Temporal Lobes in Semantic Variant Primary Progressive Aphasia and Alzheimer's Disease. *Journal*

of Korean Medical Science, *38*(41).

Landin-Romero, R., Tan, R., Hodges, J. R., & Kumfor, F. (2016). An update on semantic dementia: genetics, imaging, and pathology. *Alzheimer's research & therapy*, *8*(1), 1-9.

Lee, D. Y., Lee, K. U., Lee, J. H., Kim, K. W., Jhoo, J. H., Kim, S. Y., Yoon, J. C., Woo, S. I., Ha, J., & Woo, J. I. (2004). A normative study of the CERAD neuropsychological assessment battery in the Korean elderly. *Journal of the International Neuropsychological Society*, *10*(1), 72-81. https://www.cambridge.org/core/journals/journal-of-the-international-neuropsychological-society/article/abs/normative-study-of-the-cerad-neuropsychological-assessment-battery-in-the-korean-elderly/67046A1077EE7CA2CD41FBA2A9933360

Lee, J. H., Lee, K. U., Lee, D. Y., Kim, K. W., Jhoo, J. H., Kim, J. H., Lee, K. H., Kim, S. Y., Han, S. H., & Woo, J. I. (2002). Development of the Korean version of the Consortium to Establish a Registry for Alzheimer's Disease Assessment Packet (CERAD-K): clinical and neuropsychological assessment batteries. *J Gerontol B Psychol Sci Soc Sci*, *57*(1), P47-53. https://doi.org/10.1093/geronb/57.1.p47

Lee, S., Kim, K. W., & Initiative, A. s. D. N. (2021). Associations between texture of T1-weighted magnetic resonance imaging and radiographic pathologies in Alzheimer's disease. *European journal of neurology*, *28*(3), 735-744.

Lee, S., Lee, H., & Kim, K. W. (2020). Magnetic resonance imaging texture predicts progression to dementia due to Alzheimer disease earlier than hippocampal volume. *Journal of Psychiatry and Neuroscience*, *45*(1), 7-14.

Leigh, P., Whitwell, H., Garofalo, O., Buller, J., Swash, M., Martin, J., Gallo, J.-M., Weller, R., & Anderton, B. (1991). Ubiquitin-immunoreactive intraneuronal inclusions in amyotrophic lateral sclerosis: morphology, distribution, and specificity. *Brain*, *114*(2), 775-788.

Morris, J. C. (1993). The Clinical Dementia Rating (CDR): current version and scoring rules. *Neurology*.

Mummery, C. J., Patterson, K., Price, C. J., Ashburner, J., Frackowiak, R. S., & Hodges, J. R. (2000). A voxel-based morphometry study of semantic dementia: relationship between temporal lobe atrophy and semantic memory. *Annals of neurology*, *47*(1), 36-45.

Neary, D., Snowden, J. S., Gustafson, L., Passant, U., Stuss, D., Black, S., Freedman, M.,

Kertesz, A., Robert, P., & Albert, M. (1998). Frontotemporal lobar degeneration: a consensus on clinical diagnostic criteria. *Neurology*, *51*(6), 1546-1554.

Neary, D., Snowden, J. S., Gustafson, L., Passant, U., Stuss, D., Black, S., Freedman, M., Kertesz, A., Robert, P. H., Albert, M., Boone, K., Miller, B. L., Cummings, J., & Benson, D. F. (1998). Frontotemporal lobar degeneration: a consensus on clinical diagnostic criteria. *Neurology*, *51*(6), 1546-1554. https://doi.org/10.1212/wnl.51.6.1546

Neumann, M., Sampathu, D. M., Kwong, L. K., Truax, A. C., Micsenyi, M. C., Chou, T. T., Bruce, J., Schuck, T., Grossman, M., & Clark, C. M. (2006). Ubiquitinated TDP-43 in frontotemporal lobar degeneration and amyotrophic lateral sclerosis. *Science*, *314*(5796), 130-133.

Patel, M. B., Rodriguez, J. J., & Gmitro, A. F. (2008). Effect of gray-level re-quantization on co-occurrence based texture analysis. 2008 15th IEEE International Conference on Image Processing,

Pyun, J.-M., Park, Y. H., Kim, H.-R., Suh, J., Kang, M. J., Kim, B. J., Youn, Y. C., Jang, J.-W., Kim, S., & Initiative, A. s. D. N. (2017). Posterior atrophy predicts time to dementia in patients with amyloid-positive mild cognitive impairment. *Alzheimer's Research & Therapy*, *9*, 1-9.

Ratnavalli, E., Brayne, C., Dawson, K., & Hodges, J. (2002). The prevalence of frontotemporal dementia. *Neurology*, *58*(11), 1615-1621.

Reetz, K., Gaser, C., Klein, C., Hagenah, J., Büchel, C., Gottschalk, S., Pramstaller, P. P., Siebner, H. R., & Binkofski, F. (2009). Structural findings in the basal ganglia in genetically determined and idiopathic Parkinson's disease. *Movement Disorders*, *24*(1), 99-103.

Rogalski, E., Cobia, D., Martersteck, A., Rademaker, A., Wieneke, C., Weintraub, S., & Mesulam, M.-M. (2014). Asymmetry of cortical decline in subtypes of primary progressive aphasia. *Neurology*, *83*(13), 1184-1191. https://www.ncbi.nlm.nih.gov/pmc/articles/PMC4176026/pdf/NEUROLOGY2014583930.pdf

Rohrer, J. D., Lashley, T., Schott, J. M., Warren, J. E., Mead, S., Isaacs, A. M., Beck, J., Hardy, J., De Silva, R., & Warrington, E. (2011). Clinical and neuroanatomical signatures of tissue pathology in frontotemporal lobar degeneration. *Brain*, *134*(9), 2565-2581.

Rohrer, J. D., & Rosen, H. J. (2013). Neuroimaging in frontotemporal dementia.

International Review of Psychiatry, *25*(2), 221-229.

Scahill, R. I., Schott, J. M., Stevens, J. M., Rossor, M. N., & Fox, N. C. (2002). Mapping the evolution of regional atrophy in Alzheimer's disease: unbiased analysis of fluid-registered serial MRI. *Proceedings of the National Academy of Sciences*, *99*(7), 4703-4707.

Scheltens, P., Leys, D., Barkhof, F., Huglo, D., Weinstein, H., Vermersch, P., Kuiper, M., Steinling, M., Wolters, E. C., & Valk, J. (1992). Atrophy of medial temporal lobes on MRI in" probable" Alzheimer's disease and normal ageing: diagnostic value and neuropsychological correlates. *Journal of Neurology, Neurosurgery & Psychiatry*, *55*(10), 967-972.

Seidel, K., Bouzrou, M., Heidemann, N., Krüger, R., Schöls, L., den Dunnen, W. F., Korf, H. W., & Rüb, U. (2017). Involvement of the cerebellum in Parkinson disease and dementia with Lewy bodies. *Annals of neurology*, *81*(6), 898-903.

Snowden, J. S., Harris, J. M., Thompson, J. C., Kobylecki, C., Jones, M., Richardson, A. M., & Neary, D. (2018). Semantic dementia and the left and right temporal lobes. *Cortex*, *107*, 188-203.

Snowden, J. S., Thompson, J., & Neary, D. (2004). Knowledge of famous faces and names in semantic dementia. *Brain*, *127*(4), 860-872.

Tak, K., Lee, S., Choi, E., Suh, S. W., Oh, D. J., Moon, W., Kim, H. S., Byun, S., Bae, J. B., & Han, J. W. (2020). Magnetic resonance imaging texture of medial pulvinar in dementia with Lewy bodies. *Dementia and Geriatric Cognitive Disorders*, *49*(1), 8-15.

Teipel, S. J., Pruessner, J. C., Faltraco, F., Born, C., Rocha-Unold, M., Evans, A., Möller, H.-J., & Hampel, H. (2006). Comprehensive dissection of the medial temporal lobe in AD: measurement of hippocampus, amygdala, entorhinal, perirhinal and parahippocampal cortices using MRI. *Journal of neurology*, *253*, 794-800.

Tomé, S. O., Tsaka, G., Ronisz, A., Ospitalieri, S., Gawor, K., Gomes, L. A., Otto, M., von Arnim, C. A., Van Damme, P., & Van Den Bosch, L. (2023). TDP-43 pathology is associated with increased tau burdens and seeding. *Molecular Neurodegeneration*, *18*(1), 71.

Vijayakumar, A., & Vijayakumar, A. (2013). Comparison of hippocampal volume in dementia subtypes. *International Scholarly Research Notices*, *2013*(1), 174524.

Vos, S. J., Delvenne, A., Jack Jr, C. R., Thal, D. R., & Visser, P. J. (2024). The clinical importance of suspected non-Alzheimer disease pathophysiology. *Nature*

Reviews Neurology, 1-10.

Vos, S. J., Verhey, F., Frölich, L., Kornhuber, J., Wiltfang, J., Maier, W., Peters, O., Rüther, E., Nobili, F., & Morbelli, S. (2015). Prevalence and prognosis of Alzheimer's disease at the mild cognitive impairment stage. *Brain*, *138*(5), 1327-1338.

Winblad, B., Palmer, K., Kivipelto, M., Jelic, V., Fratiglioni, L., Wahlund, L. O., Nordberg, A., Bäckman, L., Albert, M., & Almkvist, O. (2004). Mild cognitive impairment–beyond controversies, towards a consensus: report of the International Working Group on Mild Cognitive Impairment. *Journal of internal medicine*, *256*(3), 240-246.

Wisse, L., De Flores, R., Xie, L., Das, S., McMillan, C., Trojanowski, J., Grossman, M., Lee, E., Irwin, D., & Yushkevich, P. (2021). Pathological drivers of neurodegeneration in suspected non-Alzheimer's disease pathophysiology. *Alzheimer's Research & Therapy*, *13*(1), 100.

Yoo, S.-W., Kim, Y.-S., Noh, J.-S., Oh, K.-S., Kim, C.-H., NamKoong, K., Chae, J.-H., Lee, G.-C., Jeon, S.-I., & Min, K.-J. (2006). Validity of Korean version of the mini-international neuropsychiatric interview. *Anxiety and Mood*, *2*(1), 50-55.

Zhang, Y., Moore, G. W., Laule, C., Bjarnason, T. A., Kozlowski, P., Traboulsee, A., & Li, D. K. (2013). Pathological correlates of magnetic resonance imaging texture heterogeneity in multiple sclerosis. *Annals of neurology*, *74*(1), 91-99.

국문 초록

알츠하이머병과 유사한 신경 퇴행성 질환의 탐구: 자기공명영상의 부피 및 텍스처 분석

서울대학교 대학원

뇌인지과학과

권민정

연구 배경 및 목적: 의미 치매(SD)와 비알츠하이머병 병리(SNAP)는 알츠하이머병(AD)과는 구별되는 신경 퇴행성 질환이지만, 임상적 및 신경 영상적 특징이 겹쳐 조기 진단과 치료가 어렵다. AD 진단 도구인 아밀로이드 PET 영상 및 분자 바이오 마커는 발전했으나, SD와 SNAP에 해당하는 동등한 도구는 여전히 개발이 부족하다. 구조적 MRI는 유용한 도구이지만, 기존의 부피 기반 분석만으로는 미세한 신경 퇴행 변화를 탐지하기에 한계가 있다. 뇌 조직의 미세구조 변화를 정량화하는 텍스처 분석은 질환별 신경퇴행 패턴을 보다 정교하게 이해할 수 있도록 돕는 방법으로 이 격차를 해소할 수 있다. 본 연구는 1) 텍스처 및 부피 지표를 사용해 SD와 SNAP의 신경 퇴행 패턴을 특성화하고, 2) 부피 기반, 텍스처 기반, 그리고 복합 모델의 진단 성능을 평가하며, 3) 텍스처와 부피 지표를 결합함으로써 단일 방식 모델보다 진단 정확도가 향상되는지를 확인하였다. 본 연구의 결과로 SD와 SNAP을 AD와 구별하고, 맞춤형 진단 도구와 치료 전략 개발에 기여할 것을 기대한다.

연구 방법: 본 연구는 구조적 MRI 데이터를 분석하여 SD, SNAP, AD 간 신경 퇴행 패턴을 구별하였다. 연구 1에서는 SD 환자 30명, 연령, 성별, 교육 수준을 일치시킨 AD 환자 60명, 정상 대조군(NC) 60명을 한국 노인 종단 연구(KLOSCAD)에서 등록하였다. 연구 2에서는 치매 클리닉 방문자 288명과 KLOSCAD 참여자 214명을 포함한 총 502명을 연구 대상으로 하였다. 참가자들은 18F-florbetaben PET 및 MRI를 사용하여 아밀로이드 베타 침착 및 신경 퇴행 지표를 기반으로 NC(A-N-), AD(A+N+), SNAP(A-N+) 그룹으로 분류되었다.

뇌 부피는 3D T1 강조 MRI에서 FreeSurfer를 사용하여 측정하였고, 텍스처 특징은 히스토그램 정규화, 뇌척수액(CSF) 대비 강도 정규화, 회색조 값을 균일한 범위로 재조정하는 3단계 전처리를 통해 추출하였다. 회색조 공행렬(GLCM)을 사용하여 텍스처 지표를 계산하였으며, "대비(contrast)"는 특정 뇌 영역 내의 회색조 변화와 공간적 분포를 반영하였다.

부피 및 텍스처 특징을 사용하여 분류를 위한 로지스틱 회귀 모델을 개발하고, 두 가지 방식의 유의미한 특징을 결합한 복합 모델을 제안하였다. 모델 성능은 수신자 조작 특성(ROC) 곡선 분석으로 평가되었으며, 곡선 아래 면적(AUC)을 비교하였다. 그룹 간 비교를 위한 ANCOVA와 같은 통계 분석은 SPSS와 MedCalc를 사용하여 수행되었으며, 모든 분석에서 유의 수준은 $P < 0.05$로 설정하였다.

연구 결과: 연구 1에서는 SD가 NC 및 AD와 비교하여 뚜렷한 인지 장애와

신경 퇴행 패턴을 보였다. SD 환자는 측두엽의 전두극에서 현저한 위축을 보였으며, 텍스처 분석에서 해당 부위의 미세구조 변화가 확인되었다. 로지스틱 회귀 모델은 전두극과 해마의 텍스처 특징이 SD를 NC 및 AD와 효과적으로 구별하는 데 유용함을 보여주었다. 부피와 텍스처 지표를 결합한 복합 모델은 분류 정확도를 향상시켜 SD의 미세구조 변화를 강조하였다.

연구 2에서는 SNAP과 AD가 구조적 및 미세 구조적 변화에서 뚜렷한 차이를 보였다. 텍스처 분석은 특히 시상에서 이질성이 증가한 것을 밝혀내어 SNAP을 AD와 구별할 수 있음을 보여주었다. 로지스틱 회귀 모델은 SNAP을 구별하는 데 있어 전두엽 및 피질하 텍스처 특징이 중요한 역할을 한다고 확인하였다. 부피 및 텍스처 지표를 통합한 복합 모델은 진단 성능을 향상시켰으며, SNAP에서의 미세 신경 퇴행 차이를 탐지하는 데 텍스처 분석의 유용성을 입증하였다.

결론: 본 연구는 SD와 SNAP과 같이 AD를 모방하는 신경 퇴행성 질환에서 텍스처 분석의 유용성을 보여주었다. 텍스처 분석은 초기 미세구조 변화를 탐지하여 AD와 비알츠하이머병 상태를 보다 정확하게 구별할 수 있는 유용한 진단 도구로, 조기 진단을 개선하고 맞춤형 치료 전략에 기여할 가능성을 제시한다.

키워드: 알츠하이머병, 의미 치매, 비알츠하이머병 병리, 자기공명영상, 부피, 텍스처

학번: 2020-31019